Low levels of Grainy head isoforms regulate *Drosophila* midgut intestinal stem cell differentiation.

Nicole Dominado[1], Franca Casagranda[1], Nicole A. Siddall[1], Helen E. Abud[2, 3] and Gary R. Hime[1]

1. Department of Anatomy and Neuroscience, University of Melbourne, Parkville 3010, Australia
2. Department of Anatomy and Developmental Biology, Biomedicine Discovery Institute, Monash University, Clayton 3800, Australia
3. Development and Stem Cells Program, Monash Biomedicine Discovery Institute, Monash University, Clayton, 3800, Victoria, Australia

Corresponding author:

Professor Gary Hime

Department of Anatomy and Neuroscience, The University of Melbourne, Parkville, Victoria, Australia 3010

Tel: +61-3-8344-5796

Email: g.hime@unimelb.edu.au

Final character count: 95,055 with spaces

Abstract

Regeneration of the *Drosophila* midgut epithelium depends upon differential expression of transcription factors in intestinal stem cells and their progeny. The *grainy head* locus produces multiple splice forms that result in production of two classes of transcription factor, designated Grh.O and Grh.N. *grainy head* is expressed at very low levels in the midgut and yet Grh.O is required for maintenance of intestinal stem cells and exhibits a second function regulating enteroblast differentiation in conjunction with *miR-8* and Zfh-1. Grh.O expression must be tightly regulated as high level ectopic expression in enteroblasts results in cells with confused identity and promotes excess proliferation in the epithelium. Expression of Grh.N in intestinal stem cells promotes differentiation to enterocytes. Thus midgut regeneration is not only dependent upon signalling pathways that regulate transcription factor expression, but also upon regulated mRNA splicing of these genes. This study also indicates that networks of transcription factors are acting at very low levels to regulate stem cell maintenance and differentiation.

Key words: Drosophila/ grainy head/ intestine/ stem cells

Introduction

Epithelial tissues provide barrier function between organs and their surrounds, which may comprise internal body cavities or the environment external to the organism. Most epithelia are therefore at risk of damage from biological, chemical and traumatic insult, not withstanding the deterioration due to cellular aging, and thus must be able to repair or replace damaged cells (Tai *et al*, 2019). The majority of epithelia accomplish this task by utilisation of a pool of stem cells that have the capacity to replace themselves and produce progeny that can differentiate into the specialised absorptive, secretory, structural and ciliated cells that are required in diverse epithelia.

The *Drosophila* midgut epithelium has emerged as an excellent model to study the molecular processes that regulate maintenance of epithelial stem cells and their differentiation. The midgut epithelium is surrounded by a network of oxygen providing epithelial tracheal tubes (Linneweber *et al*, 2014) followed by two layers of visceral muscle (VM), one longitudinal and the other circular (Klapper, 2000). The VM not only mediates peristalsis but also acts as a source of ligands for the overlying epithelial monolayer (Buchon *et al*, 2010, Guo *et al*, 2013, Jiang *et al*, 2009, Lin *et al*, 2008, Lin *et al*, 2010, Zhou *et al*, 2015). Between the VM and the epithelium lies the basement membrane (BM), which aids in anchoring the epithelium. The epithelium itself, contains two types of differentiated cells, the absorptive enterocyte (EC) and enteroendocrine (EE) cells. ECs are large polyploid absorptive cells that make up the bulk of the midgut epithelia. Interspersed among the ECs are the hormone producing EE cells, which are capable of regulating peristalsis (LaJeunesse *et al*, 2010), cell fate (Biteau & Jasper, 2014, Zeng *et al*, 2015) and intestinal stem cell (ISC) proliferation (Amcheslavsky *et al*, 2014, Scopelliti *et al*, 2014).

The differentiated cells of the midgut epithelium are constantly replaced by a population of regenerating ISCs. ISCs are scattered along the basal surface of the entire midgut epithelium amongst the EC and EE cells and mostly undergo asymmetric division. During this division ISCs produce a daughter ISC and a transient progenitor, an enteroblast (EB). The EB can then differentiate into either an absorptive EC or a secretory EE depending on the level of Notch signaling (Micchelli & Perrimon, 2006, Ohlstein & Spradling, 2006, Ohlstein & Spradling, 2007). Although it is established that ISCs can give rise to both ECs and EE cells, recent findings suggest that ECs and EEs arise from different progenitors with many studies now supporting the idea that EE cells originate from ISCs primed to form EE cells (Biteau & Jasper, 2014, Chen *et al*, 2018, Zeng *et al*, 2015, Zeng & Hou, 2015).

A number of conserved transcription factors have been shown to regulate ISC dynamics. These include members of the Snail family (Korzelius *et al*, 2014, Loza-Coll *et al*, 2014) which has been associated with the acquisition of stem cell properties (Mani *et al*, 2008). Exactly how *Snail* genes are differentially utilised to maintain epithelial stem cells and drive mesenchymal formation is not clear but may relate to threshold levels of expression of these transcription factors in different cell types. *Snai1* is expressed at very low levels in intestinal epithelial stem cells and their progeny in the mouse small intestine (Horvay *et al*, 2011, Horvay *et al*, 2015), yet is required to maintain the stem cell population in the base of crypts. Two members of the Snail family (Escargot and Snail) have been associated with regulation of epithelial stem cells in the *Drosophila* midgut (Dutta *et al*, 2015, Korzelius *et al*, 2014, Loza-Coll *et al*, 2014), with RNAseq data indicating that *snail* exhibits 7-10 fold lower levels of expression in ISCs and 12-19 fold lower expression in EBs in regions 4-5 of the posterior

midgut than *escargot* (Dutta *et al*, 2015). We questioned if other transcription factors that are expressed at low levels may also play significant roles in ISC regulation.

The Grainy head (Grh) family of transcriptional regulators is conserved across metazoan lineages and factors in epidermal barrier formation, wound healing, tubulogenesis and cancer. Appearance of the *grainy head* gene family coincides with the evolution of epithelia, highlighting the importance of this family for epithelial regulation (Traylor-Knowles *et al*, 2010).

The Grh family of transcription factors was originally identified in *Drosophila* with the *grainy head* gene name reflecting its mutant phenotype of a grainy head skeleton (Bray & Kafatos, 1991, Nüsslein Volhard *et al*, 1984). Since its identification in *Drosophila, grh* genes have been identified in a number of different species. *Drosophila* and *C. elegans* have a solitary *grh* gene whereas the zebrafish has evolved four *grh-like (grhl)* genes, *grhl-1, grhl-2a, grhl-2b and grhl-3.* Similarly, mice and humans have evolved three *Grhl* genes, *Grhl-1, Grhl-2* and *Grhl-3.*

Studies in both *Drosophila* and mice have demonstrated that specific Grh proteins are essential for formation and maintenance of epithelial tissues. The vertebrate studies have produced complex results with different members of the Grh family associated with induction of differentiation and in some cancer studies, stemness (Chen *et al*, 2012, Gao *et al*, 2013, Tanimizu *et al*, 2014, Tanimizu *et al*, 2013, Yu *et al*, 2009).

In *Drosophila,* the single *grh* (also known as *Elf-1* or *NTF-1)* gene is alternatively spliced. Initial investigations into *grh* splicing defined 4 mRNA transcripts, *grh.N, grh.N', grh.O and grh.O'* (Uv *et al*, 1997). However, sequencing of the entire fly genome revealed another 4 transcripts, *grh-RK, grh-RO, grh.RN and grh-RI* in addition to those originally characterized by Uv *et al* (1997), renamed as *grh-RH, grh-RP, grh-RL* and *grh-RJ* (Figure 1A). Based on the analysis of

grh mRNA transcript structures *grh* transcripts can be classed into two groups. Transcripts containing exons 4 and 5 are classed as O-isoforms whereas those without exons 4 and 5 are classed as N-isoforms (Uv *et al*, 1997) (Figure 1A). O-isoforms have been reported as being restricted to neural tissues in third instar larvae with N-isoforms associated with epithelial maintenance and wound repair in non-neural tissues (Bray & Kafatos, 1991, Mace *et al*, 2005, Uv *et al*, 1997, Wang *et al*, 2009). No studies have addressed whether Grh isoforms function in maintenance of the midgut epithelium or in any adult *Drosophila* tissue. Analysis of Grh in the midgut would facilitate an understanding of how this gene family may function in regenerative epithelia. Here we show that both isoforms are expressed at very low levels in the posterior midgut epithelium where they play different roles in regulating ISC maintenance, proliferation and differentiation.

Results

Grainy head is expressed in the adult midgut

To determine if *grh* transcripts are expressed in the adult midgut, we utilized droplet digital PCR (ddPCR) as it is a highly sensitive method that allows the absolute quantification of mRNA within a sample (Hindson *et al*, 2011). Due to the conservation of exons between *grh* transcripts (Figure 1A), primers unique to each individual transcript could not be designed, with the exception of *grh-RK* which contains a distinct exon. We therefore used primers to target subsets of *grh* mRNA transcripts (Supplementary Table 1). Additionally, primers for *esg* an ISC/EB marker (Micchelli & Perrimon, 2006) and *sna,* a gene known to function in ISC and EBs (Dutta *et al*, 2015) were used as positive controls. As expected, ddPCR conducted on adult

w^{1118} wild type midguts showed robust *esg* expression (Figure 1B) (1231 copies/μl ±318: Mean ± SEM) with expression of *sna* barely detectable at a much lower level (1.99 copies/μl ±0.96). Comparatively, primers detecting all *grh* transcripts showed an expression level of 5.60 copies/μl ±1.51. Transcripts responsible for the formation of the O-isoform expression were also detected in the midgut with the primer set detecting *grh-RL, RJ, RN and RO* showing an expression level of 0.86 copies/μl ± 0.58, comparable to the level exhibited by *sna*. Moreover, primers detecting RL and RJ showed a comparable expression level of 0.67 copies/μl ± 0.34 suggesting that the majority of O-isoform transcripts are *grh-RL and* RJ. *grh-RK* could not be detected in the midgut.

ddPCR showed *grh* transcripts are expressed in the adult midgut but did not indicate what cell type/s express Grh. To investigate the spatial resolution of Grh, immunofluorescent staining of phenotypically wild type midguts utilizing several Grh specific antibodies was carried out. However, an immunofluorescent signal could not be detected using four of the five antibodies tested (Baumgardt *et al*, 2009, Bray *et al*, 1989, Harrison *et al*, 2010, Kim & McGinnis, 2011, Nevil *et al*, 2017) (Supplementary Figure 1A-D). While an immunofluorescent signal was detected using the final Grh antibody tested, this was later shown to be a non-specific signal with the signal remaining in GFP marked *grh* null mutant clones (Supplementary Figure 1E-F). Furthermore, an immunofluorescent signal in the midgut remained undetectable in several *grh* reporter lines (Supplementary Figure 1G-K).

To further investigate the undefined expression pattern of Grh, we obtained drivers from the Janelia Collection at the Bloomington *Drosophila* Research Center that express Gal4 under the control of enhancer sequences (Pfeiffer *et al*, 2008) and used them to drive *UAS-GFP* (Supplementary Table 2). Drivers acquired use sequences within the *grh* locus to express Gal4

and may contain *grh* regulatory sequences that report the expression pattern of Grh. To amplify the expression of GFP in *grh-Gal4> UAS-GFP* midguts, adult flies were transferred to 29°C for 7 days and then immunostained using a GFP antibody. However, immunostaining of *grh-Gal4> UAS-GFP* midguts still did not reveal the expression pattern of Grh in the midgut. To further enhance the fluorescent GFP signal, Tyramide Signal Amplication (TSA) was carried out. The efficiency of TSA in amplifying a GFP signal was first tested on *grh-GFP* larval eye imaginal discs. Compared to wild type larval eye imaginal discs and non-tyramide treated *grh-GFP* larval eye discs, TSA was able to enhance the fluorescent GFP signal by approximately 10-fold (Supplementary figure 2A-E). As GFP was shown to be amplified in the larval eye disc, TSA was then also used to screen *grh-Gal4> UAS-GFP* midguts. Of the eleven *grh-Gal4* drivers screened, a TSA amplified fluorescent GFP signal was observed in two *grh-Gal4* lines driving GFP, *GMR41C09-Gal4 > UAS-GFP* and *GMR44G11-Gal4 > UAS-GFP* (Figure 1C-F, Supplementary Table 2). This signal was observed in cells with small nuclei suggesting that *grh* is expressed in either ISCs, EBs or EEs. Phenotypes observed from knockdown/out experiments in ISC and EBs (Figure 2) suggest that grainy head is intrinsically required in ISCs and EBs. No signal was observed in control midguts (Figure 1D, F) demonstrating the specificity of the assay.

Grainyhead O-isoforms are required to maintain ISCs by preventing differentiation

We designed a strategy that allowed us to investigate the overall function of Grh and the specific role of the O isoform in the adult midgut. We examined two *grh* amorphic (null) alleles, grh^{S2140} and grh^{IM}, in addition to a hypomorphic allele, grh^{370} which only disrupts O-isoform function (Uv *et al*, 1997). Homozygotes of each of these alleles are embryonic lethal, hence the MARCM system was utilized to generate GFP marked homozygous *grh* mutant

clones in posterior midgut tissue. These clones were generated via heat shock and allowed to grow for 5 to 10 days post clonal induction (DPCI) (Lee & Luo, 1999).

Initial analysis of the MARCM clones revealed that the number of *grh*^{370} clones per midgut was less than that of control and *grh* null mutant clones (Figure 2A-H). While the number of control and *grh* null mutant clones per midgut increased from 5DPCI to 10DPCI, the number of *grh*^{370} clones significantly decreased during the same time period (Figure 2I). Given that clones arise and are maintained by ISCs, a loss of GFP marked clones over time would suggest that Grh O-isoforms are required for the maintenance of ISCs. To further investigate this hypothesis, control and *grh* mutant clones 10DPCI were immunostained with the ISC marker, Delta (Dl) and the proportion of clones with at least a single Dl+ cell quantified. In comparison to controls (0.49±0.04 clones), there was a slight but non-significant decrease in the proportion of clones with at least 1 Dl+ cell in *grh* null mutants (*grh*^{S2140}*:* 0.35±0.06; *grh*^{IM}*:* 0.37±0.06 clones) (Figure 2J). In contrast, a more severe reduction was observed in the O-isoform specific mutant *grh*^{370} with only 0.10±0.03 clones containing at least one ISC.

The more severe phenotype observed in *grh*^{370} MARCM clones suggested that either loss of the O-isoform has a more severe effect than complete loss of Grh function, or that a second site mutation on the *grh*^{370} chromosome was responsible for the decrease in ISC maintenance. We therefore sought to validate the observed phenotype in two ways. Firstly, we generated another *grh* mutation *(grh*^{WG}*)* specific for O-isoforms using CRISPR (see materials and methods). The *grh*^{WG} allele was then recombined to FRT42D and the number of MARCM clones generated per midgut was quantified. Similar to the decrease observed in the number of *grh*^{370} clones, the number of *grh*^{WG} clones per midgut also decreased at 6DPCI (16.13 ± 4.55 clones) and 10DPCI (19.19 ± 3.44 clones) in comparison to controls (41.89 ± 3.54

and 44.96 ± 4.34, at 6DPCI and 10DPCI, respectively) (Supplementary Figure 3A-C). As the phenotype recapitulated what was observed with the *grh*^{370} mutation, the loss of *grh*^{WG} in MARCM clones confirms that the loss of Grh O-isoforms are responsible for the loss of ISCs and not a secondary unknown mutation in the *grh*^{370} background.

The requirement for Grh O-isoforms in maintaining ISCs was further confirmed using RNA interference. For this experiment we generated a *grh* short hairpin RNA targeting exon 5 and therefore specifically targeted O-isoforms (see materials and methods). This was then driven in ISCs and EBs using the *esg-Gal4, UAS-GFP; Tub-Gal80* (henceforth known as *esg*^{TS}) driver. After 14 days at the permissive temperature, midguts were immunostained and the proportion of Dl+ cells quantified (Figure 2K-M). Quantification of Dl+ cells in control midguts showed that there was an average proportion of 0.10 Dl+ cells of the total cells. This average proportion significantly decreased to 0.07 in *esg*^{TS} *> UAS-grh.O RNAi*. Further analyses quantifying the ratio of ISCs to EBs (by examination of the proportion of Esg+ cells that were also Dl+) show a decrease of ISCs in *esg*^{TS} *> UAS grh.O RNAi* midguts containing a mean proportion of 0.20 Dl+ cells compared to an average proportion of 0.30 Dl+ in control midguts (Figure 2N). This suggests that the majority of the relative proportion of GFP marked ISC/EBs (hereafter termed Esg+ or progenitor cells) in *esg*^{TS} *> UAS grh.O RNAi* midguts are EBs and that knock down of Grh O-isoforms results in premature differentiation of ISCs to EBs. No difference was observed using RNAi that targets all isoforms (Figure 2O-P), further indicating that it is the specific loss of Grh.O that results in loss of ISCs.

It would be expected that as *grh*^{370} mutant clones at 10DPCI have fewer ISCs they would exhibit a decrease in proliferation relative to control clones. To measure ISC proliferation, a

simple yet, effective strategy is to count the number of cells within a MARCM clone. This strategy draws on the understanding that ISCs undertake the majority of mitotic divisions in the midgut. This characteristic coupled with the reliance of the MARCM system on mitotic recombination (Lee & Luo, 1999) allows the progeny of ISCs to be lineage traced. Thus, clonal size was used as a measure of ISC proliferation in control and *grh* mutant MARCM clones (Supplementary Figure 4A). As expected, the clonal size of grh^{370} mutant clones was significantly smaller, averaging 1 cell per clone compared to control clones, which had a mean of approximately 6 cells per clone. A similar result was obtained from analysis of the grh^{WG} allele (Supplementary Figure 3D). The number of cells per clone also significantly decreased in *grh* null mutant clones (mean of ~4 cells per clone) when compared to controls. Although, *grh* null mutant clones had fewer cells they were still capable of forming multicellular clones.

Multicellular *grh* null clones were often composed of cells with varying nuclear sizes. This suggested that these clones were composed of a variety of different cell types. To distinguish the cell types that make up *grh* mutant clones, the EC marker Pdm-1 and the EE marker Prospero (Pros) were assayed in control and *grh* mutant MARCM clones (Supplementary Figure 4B). The percentages of cells within clones with an EC fate (Pdm-1+ GFP+), EE fate (Pros+ GFP+) and an ISC/EB fate (GFP+ only) were quantified. The cellular composition between control and *grh* null mutant clones (Supplementary Figure 4B) was similar (ECs: 25-31%, EEs: 5-6% and ISC/EBs: 63-69%) suggesting that the complete loss of Grh does not affect differentiation. The specific loss of the O-isoforms also did not prevent differentiation as grh^{370} cells positive for EC marker, Pdm-1 (4% of homozygous grh^{370} mutant cells) and EE marker, Pros (9% of homozygous grh^{370} mutant cells) could be detected, albeit Pdm-1 was

detected at a much lower percentage than in control clones. Consequently, an increase in ISC/EBs (87% of *grh*^{370} homozygous mutant cells) was observed. As it has previously been shown that loss of Grh O-isoforms results in a loss of ISCs, it is likely that a majority of these GFP+ only cells are EBs. These data imply that loss of O-isoform function results in differentiation of ISCs to EBs but also a reduced rate of EB to EC differentiation.

As differentiation did not appear to be affected in *grh* null mutant clones, it was hypothesized that Grh may have a separate function in the mature midgut epithelium. The epithelial monolayer lining the midgut acts as a critical barrier to the external environment with barrier dysfunction linked to fly mortality (Clark *et al*, 2015, Rera *et al*, 2012). Barrier integrity relies upon close cell-cell adhesion achieved by the expression of junctional proteins. Several junctional proteins including Coracle (Cora), Fasciclin III and *Drosophila* E-Cadherin (DE-Cad) have been characterized as Grh targets (Almeida & Bray, 2005, Narasimha *et al*, 2008). Therefore, to investigate if Grh regulates the expression of junctional proteins in the midgut, 10DPCI control and *grh* null mutant clones were immunostained for junctional proteins Cora and Discs Large (Dlg). Additionally, control and *grh* mutant clones were also stained for Armadillo (Arm), the *Drosophila* β-catenin and DE-Cadherin intracellular binding partner (Aberle *et al*, 1994). A fluorescence ratio was then calculated by measuring the intensity of each protein in GFP marked clones and dividing it by the fluorescence intensity of the protein in the adjacent non-clonal tissue. This serves as an internal control that minimizes any variation caused by immunostaining techniques. Quantification of fluorescence ratios showed that there was no change in the intensity of all three proteins in control or *grh* null clones all having a mean fluorescence ratio of ~1 (Supplementary Figure 5). The lack of a change in intensity suggests that the loss of Grh does not affect the expression and regulation of these

junctional proteins. It is possible that the loss of only *grh* O-isoforms may affect junctional proteins however, *grh*^{370} MARCM clones were rarely observed and were often single cell clones.

Ectopic expression of N isoforms results in differentiation

The more severe phenotype observed in O-isoform specific mutants, *grh*^{370} *and grh*^{WG} could be explained by an antagonistic interaction between the N-specific and O-specific Grh isoforms in regulating ISC function. In O-specific mutant cells, Grh N-isoforms remain which may result in increased N-isoform activity and a loss of ISCs. To test if increased N-isoform activity results in a reduced number of ISCs, a *UAS-grh.RP* isoform (produces the same protein as *grh.RI*) was over expressed in ISC/EBs using *esg*^{TS}*.* After two days at the permissive temperature, there was a significant reduction in the relative proportion of Esg+ (or progenitor cells) in *esg*^{TS} > *UAS-grh.RP* midguts compared to control midguts (Figure 3A-B & E). Likewise, ectopic expression of another N-isoform, *UAS-grh.RH* also resulted in a loss of esg+ cells (Figure 3F). Thus, ectopic expression of Grh N-isoforms in ISC/EBs results in the loss of ISC/EBs.

To investigate if the reduction of ISC/EB number due to the over expression of *grh.RP* is a result of cell death, control and *esg*^{TS} > *UAS-grh.RP* midguts were immunostained with an antibody generated against human activated Caspase 3, which also detects apoptotic cells in *Drosophila* (Fan & Bergmann, 2010, Fogarty & Bergmann, 2014). An activated Caspase 3 signal was not detected in control and *esg*^{TS} > *UAS-grh.RP* midguts suggesting that apoptosis is not the cause of ISC/EB loss (Supplementary Figure 6B). This was further confirmed by co-expressing the apoptotic inhibitor P35 (Hay *et al*, 1994) with *UAS-grh.RP* using the esg^{TS} driver

(Figure 3C-E). Co-expression of P35 with *grh.RP* for two days at the permissive temperature was not sufficient in preventing the loss of Esg+ cells with the total proportion remaining at a similar level to the expression of *grh.RP* alone. The ISC/EB proportion in midguts only expressing P35 was comparable to controls demonstrating that expression of P35 does not affect ISC/EB number. Together these data illustrate that loss of ISC/EBs due to *grh.RP* over expression is not a consequence of apoptosis.

Another possible cause for ISC/EB loss in cells that ectopically express *grh.RP* is premature differentiation. The few cells present that ectopically express *grh.RP* have large nuclei characteristic of ECs suggesting that they have all undergone differentiation (Figure 3H). Therefore, control and esg^{TS} *>UAS-grh.RP* midguts were immunostained for the EC marker, Pdm-1 and the proportion of Esg+ cells expressing Pdm-1 quantified. In comparison to control midguts, there was an increase in the proportion of Esg+ cells expressing Pdm-1 in midguts ectopically expressing *grh.RP* in ISC/EBs (Figure 3K). While this trend was also observed when *grh.RH* was ectopically expressed using esg^{TS}, quantification showed that it was not statistically significant. These data indicate that increased expression of N-isoforms in ISC and EBs induces the process of differentiation down the EC lineage.

Grh O-isoforms promote delay in differentiation that results in cells having characteristics of EBs and ECs

As the ectopic expression of N-isoforms phenocopies results observed in grh^{370} MARCM clones, we hypothesized that different Grh isoforms may have opposing roles. Since we were unable to eliminate N-isoform expression without affecting O-isoforms, we instead ectopically expressed *grh-RL,* a transcript that forms an O-isoform, in ISC and EBs using the esg^{TS} driver. Increased expression of *grh.RL* isoform in ISC/EBs resulted in an increase in the

proportion of Esg+ cells when compared to control midguts (Figure 4A-C). This could represent an increase in either ISCs or EBs, but notably the cells appeared abnormally large and elongated. To differentiate the two cell types, control and *esg^{TS} > UAS-grh.RL* midguts were immunostained with Dl. In these midguts, ISCs could be identified by the expression of both Dl and GFP while EBs would express GFP alone. While the analysis of control midguts showed the expected pattern of Dl expression, analysis of *esg^{TS} > UAS-grh.RL* midguts revealed that the majority of Esg+ cells were stained with Dl suggesting an increase in ISCs (Figure 4A-B). Interestingly, cells labelled with both Dl and GFP in *esg^{TS} > UAS-grh.RL* midguts appeared enlarged (compared to ISCs), a property of ECs which undergo endoreplication and an increase in cellular size. Therefore, to determine if these larger cells had undergone differentiation, Pdm-1 was used to stain control and *esg^{TS} > UAS-grh.RL* midguts. While Esg+ cells expressing Pdm-1 were not observed in control midguts, they were commonly observed in *esg^{TS} > UAS-grh.RL* midguts (Figure 3J-K). The expression of Pdm-1 in these *esg^{TS} > UAS-grh.RL* cells indicates that increased Grh.RL activity also induces differentiation, although the maintenance of Dl expression indicates that the cells can only partially differentiate.

The accumulation of progenitor cells with confused identity is reminiscent to the age related decline in epithelial structure and exposure to noxious chemicals that leads to cell death (Biteau *et al*, 2008). In order to investigate if ectopically expressing *grh.RL* in ISC/EBs induces cell death, caspase activity was analysed in *esg^{TS}> UAS-grh.RL* midguts (Supplementary Figure 6C). Whereas activated caspase expression was not detected in control midguts, it was detected in *esg^{TS}> UAS-grh.RL* midguts demonstrating that cell death is induced by increasing *grh.RL* expression in progenitor cells. Typically, the induction of apoptosis in the midgut leads to compensatory ISC proliferation (Liang *et al*, 2017). This was indeed observed in midguts

over expressing *grh.RL* with the mitotic index, measured by counting the number of Phospho-histone 3 positive cells, increasing to a mean of 7 compared to a control mean of 1 (Figure 4D). Moreover, the increase in mitotic index was rescued (returning to a mean of ~1) when apoptotic inhibitor P35 was co-expressed with *grh.RL*. Taken together, these suggest that over expression of *grh.RL* in ISC and EBs results in cells with confused identity and ultimately cell death. Consequently, it is cell death rather than *grh.RL* expression in ISC and EBs that stimulates ISC proliferation.

The confused identity seen in *esg^{TS}> UAS-grh.RL* midguts suggests that over expression of *grh.RL* can induce differentiation and maintenance of ISC identity. The results presented in Supplementary Figure 4B suggest that the O-isoform is required to prevent ISC differentiation to EBs, but also to enhance EB to EC differentiation. *esg^{TS}> UAS-grh.RL* results in O-isoform overexpression in both ISCs and EBs suggesting a combination of these functions may be observed in Figure 4B. In order to determine the effect of *grh.RL* overexpression in ISCs alone, *grh.RL* was ectopically expressed using *esg-Gal4, UAS-YFP; Su(H)-Gal80, Tub-Gal80^{TS}* (hereafter termed *ISC^{TS}*) which will inhibit Gal4 mediated expression in EBs. Ectopic expression of *grh.RL* in ISCs did not result in an increase in ISC number with the number of ISCs remaining at an equivalent level to that of controls (Figure 4G). Moreover, the increase in Grh.RL expression did not cause premature differentiation into ECs as GFP+ nuclear size remained at a similar size to that of controls (Figure 4E-F).

The function of Grh.RL in EBs was similarly investigated by over-expressing *grh.RL* using *Su(H)GBE-Gal4, UAS-GFP; Tub-Gal80^{TS}* (hereafter termed *Su(H)^{TS}*). Ectopic expression of *grh.RL* in EBs led to an increase in the proportion of GFP+ EBs in comparison to controls (Figure

4H). The increase in EB number appears to be as a result of an increase in the mitotic index of *Su(H)^{TS} > UAS-grh.RL* midguts (Figure 4I-K). Somewhat surprisingly, a number of these mitotically active cells were GFP+ suggesting that ectopic expression of *grh.RL* in EBs may facilitate EB cell division (Figure 4J & L). Given that cell division within the midgut is characteristic of ISC identity, it is possible that these EBs may still hold ISC-like identity. Indeed, the analysis of *Su(H)^{TS} > UAS-grh.RL* midguts marked with Dl and pH3 showed that GFP+ cells, positive for pH3 were also positive for Dl indicating that these dividing EBs also have at least a partial ISC identity.

In addition to maintaining ISC identity in *esg^{TS}> UAS-grh.RL* midguts, the over-expression of Grh.RL was also able to induce differentiation into the EC lineage. This ability was also investigated in EBs. Analysis of *Su(H)^{TS} > UAS-grh.RL* midguts showed that there was an increase in the number of EBs expressing the EC marker, Pdm-1 (Figure 4M-O) suggesting that *grh.RL* is also able to induce EB differentiation to ECs.

Grh O-isoforms interact with *microRNA-8* and Zfh-1

Antonello et al. (2015) showed that the process of EB terminal differentiation into ECs required *microRNA-8* (*miR-8*) upregulation in order to silence *esg* activity. Moreover, Antonello et al. (2015) showed the transcription factor, Zfh-1 to act upstream of Esg to maintain the mesenchymal characteristics of EBs. This intricate network is of particular interest as *grh* orthologue *Grhl-2* has been shown to suppress *zfh-1* orthologue *Zeb1* and activate *miR-8* orthologue, *miR-200* (Chung *et al*, 2016). Hence, to determine if this interaction is conserved in *Drosophila* and if *grh.RL* is able to induce differentiation in a similar capacity, we examined genetic interactions between these genes. To test if ectopic *grh.RL* is able to activate *miR-8*, *esg^{TS}* was used to co-express Grh.RL with a *miR-8* “sponge”, which

depletes *miR-8* activity (Figure 5A-E). If grh.RL activates *miR-8*, it would be anticipated that expression of the *miR-8* "sponge" would rescue the *esg^{TS}> UAS-grh.RL* over expression phenotype. As expected, co-expression of *miR-8* sponge with Grh.RL resulted in these midguts (Figure 5E) phenotypically resembling that of controls (Figure 5A) and *esg^{TS}> UAS-miR-8.sponge; UAS-grh.RL* midguts no longer displaying enlarged cells characteristic of differentiated ECs (Figure 5H). Moreover, the proportion of Esg+ cells in midguts co-expressing Grh.RL and the *miR-8* sponge decreased to control levels (Figure 5G), suggesting that Grh.RL activates *miR-8* expression in ISC/EBs.

To determine if Zfh-1 is able to influence the *esg^{TS}> UAS-grh.RL* phenotype, Grh.RL was expressed in combination with Zfh-1 (Figure 5A-F). The co-expression of both Zfh-1 and Grh.RL in Esg+ cells (Figure 5F) resulted in the rescue of the phenotype observed from expression of Grh.RL alone (Figure 5B). Whereas *esg^{TS}> UAS-grh.RL* midguts have increased numbers of Esg+ cells, the proportion of Esg+ cells in midguts expressing both Zfh-1 and Grh.RL resembled that of control and *esg^{TS}>UAS-zfh1* midguts (Figure 5G). In addition, the cell size of *esg^{TS}>UAS-zfh1; UAS-grh.RL* cells resembled that of control midguts (Figure 5H) demonstrating that Grh.RL and Zfh-1 are able to interact to regulate the differentiation of EBs.

Discussion

The regulation of ISC maintenance involves multiple molecular pathways and a network of transcription factors. In this study we have provided evidence that the transcription factor Grh is required to maintain ISCs in the *Drosophila* midgut. Interestingly, it is the function of the Grh O-isoforms, previously characterized as neural specific in the third instar larvae (Uv

et al, 1997), that is crucial for ISC maintenance. Generation of *grh*^{370} midgut clones demonstrated that Dl+ ISCs that cannot express an O-isoform isoform are lost from the epithelium. Clones arising from O-specific mutant ISCs cannot regenerate and are not maintained over time, further showing the need for the O-isoform in maintaining ISC identity and function. Specific knockdown of the O-isoform via RNA interference directed against exon 5 also resulted in a loss of Dl+ cells.

RNA interference mediated reduction of all isoforms or establishment of null clones did not result in a significant loss of ISCs. It is very unusual for a hypomorphic mutation to exhibit a more severe phenotype than a null and this result persuaded us to generate a new O-specific allele via CRISPR (*grh*^{WG}) to control for the possibility that a background mutation on the *grh*^{370} chromosome was associated with the observed phenotype. This allele behaved similarly to *grh*^{370}, and together with the RNAi data, indicates that loss of the O-isoform has a much greater effect on ISC maintenance and proliferation than complete loss of gene function. Though unusual, this sort of effect is not unprecedented and can be the result of different protein products of a gene acting in opposing manners. For example, the murine *Trp73* gene encodes multiple protein isoforms that are members of the p53 family of transcriptional regulators. The protein isoforms result from alternative mRNA splicing and use of two different transcript initiation sites (Murray-Zmijewski *et al*, 2006). Two major groups of protein isoforms result from the alternative initiation sites and are termed TAp73 and ΔNp73. TAp73 has been associated with proapoptotic activities and ΔNp73 with anti-apoptotic properties (Grob *et al*, 2001, Muller *et al*, 2005, Wang *et al*, 2007). p53 family proteins act as tetramers so incorporation of either isoform group can affect the function of the complex. Each isoform has unique properties and it appears to be the balance of isoforms in a cell that is important to determine phenotypic outcome. Specific genetic knockouts of TA,

ΔN and all isoforms have been generated in mice and each exhibits a unique phenotype. TAp73$^{-/-}$ animals develop spontaneous tumours but this is not observed in *Trp73*$^{-/-}$ nulls (Tomasini *et al*, 2008). This may not be surprising given the opposing functions of TA and ΔN isoforms but it is a another situation where a hypomorphic allele exhibits a phenotype not observed in the null.

Loss of the Grh O-isoform has the effect of producing an imbalance of products from *the grh* gene. If a similar antagonistic relationship exists between Grh O- and N-isoforms it would be expected that overexpression of the N-isoform would generate a similar phenotype to loss of the O-isoform. Overexpression of the N-isoform in ISCs and EBs resulted in a loss of ISC and EBs via forced differentiation. However, differentiation proceeded in *grh* null clones. This suggests that the N-isoform, while it may facilitate differentiation, is not critical in the absence of O-isoforms and other factors may be able to compensate for its loss.

Two other studies of transcription factor function in the *Drosophila* midgut have reported isoform-specific regulation of differentiation (Al Hayek *et al*, 2019, Tang *et al*, 2018). The POU/Oct transcription factor Nubbin/Pdm1 is expressed in enterocytes (Lee *et al*, 2009) and has been reported to repress *escargot* expression during EC differentiation (Korzelius *et al*, 2014). Two transcripts of *nubbin* are known to be expressed from alternative promoters, *nub-RB* and *nub-RD* (Dantoft *et al*, 2013, Lindberg *et al*, 2018) resulting production of 103.9 kDa Nub-PD and smaller 65.2 kDa Nub-PB protein isoforms. Nub-PD has been shown to be a repressor, acting to repress escargot in EBs/early ECs (Korzelius *et al*, 2014) and immune and stress response genes in ECs (Dantoft *et al*, 2013, Dantoft *et al*, 2016). More recently *nubbin* was shown to be expressed in ISCs/EBs and loss of Nub-PB from these cells results in failure of differentiation and hyperplasia. In contrast, loss of Nub-PD from ISCs resulted in a failure

of cell proliferation implying that Nub-PD and Nub-PC act in opposing manners (Tang *et al*, 2018). Antibodies that distinguish the two isoforms are not available however, using a similar strategy to that we employed to examine *grh* expression in the midgut, Gal4 lines that were driven either by endogenous insertions into the *nub* locus, or by DNA fragments from within the *nub* gene were able to show that both isoforms are expressed within ISC/EBs (Tang *et al*, 2018). One surprising finding from this study is that overexpression of *nub-RD* in MARCM clones did not drive ISC proliferation but instead resulted in their differentiation. This runs counter to the concept of opposing functions of the isoforms unless concentration of Nub-RD is critical for correct function, as has been reported for the Nub orthologue, OCT-4 in regulation of embryonic stem cell renewal (Niwa *et al*, 2000). Complete loss of function nub^{E37} MARCM midgut clones resemble wildtype controls compared to nub^{1} (Nub-PD mutant) which exhibit a dramatic decrease in proliferation (Tang *et al*, 2018). This again shows similarity to the *grh* phenotypes described here and suggests that the absence of *nub* can be compensated by another gene, perhaps the *Pdm2* paralogue, but the unbalanced isoform expression observed in the nub^{1} allele results in a loss of the ability to maintain ISCs.

The Ovo/Shavenbaby (Svb) transcription factor has been shown to be required for maintenance of renal nephric stem cells (Bohere *et al*, 2018) and a recent preprint describes loss of Svb in ISCs/EBs results in loss of progenitor cells via apoptosis (Al Hayek *et al*, 2019). Svb is translated into a long isoform transcriptional repressor (Svb^{REP}) and is also post-translationally processed into a short activator (Svb^{ACT}) via short peptides produced by the Polished rice (Pri) locus (Kondo *et al*, 2010, Zanet *et al*, 2015). In this case there may not be direct antagonism between Svb isoforms as Pri is expressed in ISCs/EBs where it results in production of Svb^{ACT} which functions to promote ISC proliferation, whereas Svb^{REP} is

expressed in ECs and promotes differentiation. Although, Svb^{REP} forces differentiation even when expressed in a genetic background that favours stem cell proliferation (Al Hayek *et al*, 2019).

Overexpression of the O-isoform in ISCs/EBs using esg^{TS} resulted in cells with confused identities. While a majority of the *esg+* cells expressed the ISC marker, Dl, they also exhibited increased cell size and expressed the EC marker, Pdm-1. This suggested a role for O-isoforms in both ISC maintenance and differentiation. It is possible that the high level of ectopic expression produced by GAL4 overrides the nature of the isoform being expressed but the phenotype observed with ectopic Grh.O was qualitatively different to that from Grh.N. The suppression of the ectopic Grh.O phenotype via downregulation of *miR-8* activity (via expression of a *miR-8* sponge) also suggests that O-isoforms may have an endogenous role in late EBs that is normally regulated by *miR-8*. Previous work has demonstrated that *miR-8* functions in late EBs to downregulate Escargot function and facilitate differentiation (Antonello *et al*, 2015) and we suggest that Grh O-isoforms are also part of this regulatory network. The suppression that we observed with ectopic expression of Zfh-1 also suggests that the Grh, *miR-200*, Zeb1 regulatory network that functions to maintain an epithelial phenotype in ovarian cancer cells (Chung *et al*, 2016) is an evolutionarily conserved regulatory mechanism.

The dual role of Grh.O was also observed when this isoform was specifically expressed in EBs as it resulted in EBs that express both Pdm-1 and Dl. Interestingly, over-expression of Grh.O in ISCs did not induce an increase in ISC number suggesting that it may play a role in maintaining identity rather than specifying it. The ability of Grh to maintain a stem cell population has previously been observed in the larval central nervous system (CNS). In the

larval CNS, thoracic neuroblasts (NB) are maintained by the ability of Grh to prevent programmed cell death (Cenci & Gould, 2005). Unlike the larval NB, in the midgut Grh does not appear to maintain ISCs by preventing apoptosis. Thus, Grh must use another mechanism to maintain ISCs. *grh*^{370} clones lose stem cells but increase the proportion of GFP+ Pdm-1- Pros- cells compared with control clones suggesting that they have an increased proportion of EBs, or that ISCs differentiate rather than being lost via apoptosis. These data imply that Grh O-isoforms maintain ISCs by preventing them from prematurely differentiating. The data also indicate a decrease in the proportion of GFP+ Pdm-1+ cells in *grh*^{370} clones, suggesting that the accumulated EBs have an impaired ability to differentiate into ECs, again suggesting a dual role for Grh O-isoforms to 1) maintain the ISC state, and 2) to facilitate EB to EC differentiation.

A reiterative, but different, function for Grh O-isoforms in two stages of the ISC to EC differentiation process may also explain why *grh* is expressed at such low levels in the midgut. A very tight control of *grh* expression would permit function in ISCs, which may be accompanied by a transient reduction to permit EB differentiation and subsequent upregulation to allow differentiation to ECs. To fully examine this hypothesis will require development of protocols to examine *in situ* expression of very low-level gene or protein expression during ISC and EB differentiation. It is already clear that early EBs can be distinguished from later EBs based on morphology and gene expression. *miR-8* expression is upregulated in late EBs and appears to be important for regulating levels of Escargot in order to facilitate EB transition to a fully epithelial state (Antonello *et al*, 2015). Grh may be another transcription factor that is dynamically expressed during the ISC to EB to EC transitions. Downregulation of *zfh-1* also results in enhanced EC differentiation (Antonello *et al*, 2015)

and yet according to the RNAseq data from (Dutta *et al*, 2015), available for interrogation at http://flygutseq.buchonlab.com/, *zfh-1* is expressed at even lower levels than *grh* in ISCs/EBs. It is thus highly likely that a network of interacting transcriptional regulators are acting to facilitate midgut differentiation that may be at, or beyond, the resolution of detection by current RNAseq pipelines. This underscores the importance of genetic screens that may be capable of detecting phenotypes associated with genes that could be potentially ignored from transcriptome analyses.

How Grh is able to exert its influence on intestinal regeneration could be through it's ability to activate and repress target genes. During early embryonic development, Grh represses target genes such as *decapentaplegic* and *zernullt (Huang et al, 1995, Liaw et al, 1995)*. Later in development, Grh is able to switch to a transcriptional activator, activating genes such as *Ultrabithorax, Dopa decarboxylase (Ddc)* and *fushi tarazu* (Bray & Kafatos, 1991, Dynlacht *et al*, 1989, Nevil *et al*, 2017). Grh's ability to switch from an activator to a repressor is only beginning to be elucidated.

Recent CHiP-seq and RNA-seq studies show that Grh binding does not change over several stages of embryonic development (Nevil *et al*, 2017). Yet, Grh is able to switch from a repressor to an activator. One hypothesis posited by Nevil *et al* (2017) is that Grh may act as a pioneer factor. This was later supported by Jacobs *et al* (2018) using ATAC-seq to show that Grh binding is able regulate chromatin accessibility. Functional studies whereby a Grh N-isoform was ectopically expressed in larval eye disc showed that Grh was able to bind and open closed chromatin, making targets accessible (Jacobs *et al*, 2018). Although Grh binding allows enhancer access, it is unable to activate the enhancer without the recruitment of co-factors (Jacobs *et al*, 2018). In addition to identification by Jacobs *et al* (2018) of Atonal as a

Grh co-activator, Grh is also able to form complexes with Polycomb proteins Pleiohomeotic and Dring (Blastyak *et al*, 2006, Tuckfield *et al*, 2002) further illustrating the ability of Grh to recruit co-factors to confer its activator or repressive functions. Grh's pioneer factor activity appears to be regulated temporally with Grh pioneer factor activity required during late embryonic development but not during early embryonic development (Nevil *et al*, 2020), thus whether Grh is acting as a pioneer factor or directly activating or repressing genes in the intestine requires further investigation.

The different activities of Grh.O and Grh.N isoforms could be associated with activation of isoform specific targets. There is some evidence to suggest differential target utilization as reporter genes generated by placing two different Grh-binding elements, derived from the *Ddc* gene, upstream of *LacZ* exhibit different patterns of expression in embryos (Uv *et al*, 1997). The *be1* element drives expression all cells known to express Grh whereas *be2* is specific to the central nervous system. Grh protein can be detected in optic lobes and NBs of the wildtype larval CNS but in tissue derived from homozygotes of the Grh.O-specific grh^{370} allele expression is absent from NBs while still present in optic lobes. Moreover, the *be1* reporter is expressed in optic lobes and NBs but the *be2* reporter is specific to NBs and this expression is absent in grh^{370} mutant tissue (Uv *et al*, 1997). Grh has been associated with different gene names and one of the earliest studies of function, where is was referred to as NTF-1, demonstrated it bound to target sequences as a dimer (Attardi & Tjian, 1993). In this study NTF-1 protein was produced from a cDNA we would now refer to as encoding a Grh.N isoform (Dynlacht *et al*, 1989). *be1* is a palindromic sequence but *be2* is non-palindromic (Uv *et al*, 1997) so it is possible that Grh.N binds targets as a dimer and Grh.O binds as a heterodimer, either with Grh.N or another transcriptional regulator, thereby resulting in

isoform specific gene regulation. We have been unable to find any specific homology between the O-specific exons and other protein sequences so the mechanism of how Grh.O exerts its specificity is yet to be determined. This exon does not appear to be conserved in vertebrate GRHL proteins despite them exhibiting some differential splicing (Miles *et al*, 2017) however differential activities of the vertebrate proteins offer the suggestion that isoform specific functions observed in *Drosophila* have evolved into separate gene functions in vertebrates. This is exemplified in a number of studies that have examined GRHL function in tumorigenesis. Several studies have implicated GRHL proteins in a range of cancers including neuroblastomas, skin, breast, ovarian, gastric and cervical cancers. Depending on the cancer type, GRHL proteins appear to have oncogenic or tumor suppressive roles. In breast and ovarian cancer cell lines, GRHL2 acts as a suppressor of EMT with functional studies resulting in the induction of epithelial genes, the repression of mesenchymal genes and inhibition of tumor cell motility and invasion (Chung *et al*, 2016, Cieply *et al*, 2013, Cieply *et al*, 2012). The action of GRHL2 as a suppressor of EMT is further exemplified by its low expression in cancers which have undergone EMT such as invasive mammary tumors (Werner *et al*, 2013) and ovarian cancer cells with mesenchymal signatures (Chung *et al*, 2016). The mechanism by which GRHL2 is able to inhibit EMT involves a negative feedback loop whereby GRHL2 inhibits Zeb1, a factor central to EMT (Zheng & Kang, 2014). In breast cancer, GRHL2 is able to inhibit Zeb1 directly by binding to its promoter and inhibiting Homeodomain proteins required to activate Zeb1 (Cieply *et al*, 2013, Cieply *et al*, 2012). Moreover, GRHL2 transcriptional activation of *miR-200*, another Zeb1 inhibitor, allows the indirect suppression of Zeb1 (Chung *et al*, 2016, Gregory *et al*, 2008). This negative feedback loop is completed by the ability of Zeb1 to interact with the GRHL2 promoter to inhibit its function (Cieply *et al*, 2013) suggesting a balance between the two factors regulates EMT and its reverse process MET.

More recently, GRHL2 has also been shown to also have a reciprocal relationship with Zeb1 in colorectal cancer (CRC). In a pair of studies, Quan *et al* (2014) and Quan *et al* (2015) showed GRHL2 to be upregulated in CRC samples and that this upregulation correlated with tumor progression and advanced clinical stage. This suggests an oncogenic role for GRHL2 in CRC. This oncogenic role is underlined by functional studies overexpressing GRHL2 in CRC cells lines, which induced cellular proliferation (Quan *et al*, 2015). Increased cellular proliferation induced by GRHL2 in CRC cell lines correlates with the repression of Zeb1. Knockdown of GRHL2 in CRC cell lines impairs cell proliferation and increases Zeb1 expression (Quan *et al*, 2014). Cell proliferation is restored upon transient Zeb1 knockdown in CRC cells where GRHL2 has also been silenced. Moreover, GRHL2 expression is upregulated upon Zeb1 knockdown suggesting that the reciprocal relationship between Zeb1 and GRHL2 is conserved among various cancers. Converse to the oncogenic function of GRHL2, GRHL3 can act as a tumour suppressor as loss of GRHL3 in keratinocytes suppresses Pten expression leading to subsequent activation of PI3K/AKT/mTOR signaling resulting in squamous cell carcinoma (Bhandari *et al*, 2013). GRHL1 loss has also been associated with squamous cell carcinoma formation in a mouse chemically-induced skin cancer model (Mlacki *et al*, 2014). These examples of differential effects of GRHL proteins upon tumour formation and progression may be associated with different contexts of GRHL expression or may represent divergence of GRHL function, similarly to the *Drosophila* Grh isoforms. In either case it is likely that the GRHL proteins are interacting with different cofactors to exert different effects upon tumourigenesis. The network of GRHL2 interactions illustrate that the ZEB1/Zfh1 - GRHL2/Grh - *miR-200*/*miR-8* axis appears to be conserved between *Drosophila* and mammals and further work will determine if differential effects of GRHL proteins also co-operate in regulating stem cell maintenance and differentiation in vertebrate epithelia.

Materials and Methods

Drosophila Stocks and Husbandry

Fly stocks were maintained on a standard culture medium at 25°C unless otherwise specified. Mated female flies were exclusively analysed throughout this study, due to differences in male and female ISC behavior (Hudry *et al*, 2016). A detailed list of fly strains used in this study are listed in Supplementary Table 3. Flies containing the *Tub-Gal80*^{TS} allele were crossed and maintained at the non-permissive temperature of 18°C. Following eclosion, 3-5-day old flies were transferred to the permissive temperature of 29°C for further analysis.

Generation of Marked Clones

The Mosaic Analysis with Repressible Cell Marker System (MARCM) was used to generate positively marked GFP homozygous clones. Unless otherwise stated, MARCM crosses were established and maintained at 18°C. 3-5 day old adult flies of the genotypes *UAS-cd8 GFP, hs-FLP/ +; frt42DtubGal80/ frt42D; tub-Gal4/+, UAS-cd8 GFP, hs-FLP/ +; frt42DtubGal80/ frt42Dgrh*^{S2140}*; tub-Gal4/+, UAS-cd8 GFP, hs-FLP/ +; frt42DtubGal80/ frt42Dgrh*^{IM}*; tub-Gal4/+, UAS-cd8 GFP, hs-FLP/ +; frt42DtubGal80/ frt42Dgrh*^{370}*; tub-Gal4/+* were heat shocked for 1 hour in a 37°C running water bath. Flies were then returned to 18°C to minimize the incidence of leaky MARCM clones. Intestines were analyzed 5-10 days after clonal induction.

Generation of *UAS-grh.O* RNAi Line

Short hairpin design was conducted using *grh* exon 5 sequence with top candidate selected using DSIR website (Vert *et al*, 2006). Selected hairpin, 5'-CGGGATCAGACAAATATCCAA-3' was cloned into pWALIUM20 (Ni *et al*, 2011) with potential plasmids verified by Sanger sequencing. Verified plasmid was then injected into embryos (BestGene Inc. Co) and a stable transgenic line made.

Generation of grh^{WG} allele

CRISPR mediated mutagenesis, performed by WellGenetics Inc. was used to insert 3-frame stop codons in *grh* exon 5 to generate a C-terminal truncation only affecting O-isoforms (*grh-RJ, RL, RN and RO)*. Briefly, DNA plasmids containing hs-Cas9, *grh* gRNAs targeting exon 5 and a cassette containing 2 loxP sites, selection marker 3xP3-RFP, two homology arms and 3-frame stop codons were injected into w^{1118} embryos. F1 flies carrying 3xP3-RFP selection marker were then validated by PCR, sequencing and backcrossing to grh^{IM} and *Df(grh)*.

Immunostaining

Adult mated female *Drosophila* midguts were dissected in Phosphate Buffered Saline (PBSx1). Dissected midguts were then fixed in 4% formaldehyde for 1 hour or overnight at 4°C. Following fixation, midguts were then washed 3x in PBT (PBS + 0.1% Triton-X100) for 5 minutes each and blocked for 1 hour in PBTH (PBS + 0.1% Triton X100 + 5% Horse Serum). Midguts were then incubated in the following primary antibodies: chicken anti-GFP (1:2000,

AbCam), mouse anti-Delta (1:100, DSHB), rabbit anti-Pdm-1 (1:2000, Xiaohang Yang), rabbit anti-pH3 (1:5000, Upstate), mouse anti-β-Galactosidase (1: 20, DSHB), chicken anti-β-Galactosidase (1:2000, AbCam), rabbit anti-β-Galactosidase (1:2000, Cappel), mouse anti-GRH (1:5, Sarah Bray), rat anti-GRH (1:500, Stefan Thor), rabbit anti-GRH (1:200, William McGinnis /1:1000, Melissa Harrison), rabbit anti-Activated Caspase 3 (D175) (1: 200, Cell Signaling Technologies), mouse anti-Cora (1:20, DSHB) and mouse anti-Dlg (1: 20, DSHB) overnight at 4°C. After primary antibody incubation, the samples were washed 3x for 5 minutes in PBT and incubated in corresponding Alexa Fluor (1:500, Invitrogen) secondary antibodies for 2 hours. This was then followed by a DAPI wash for 20 minutes and 3x washes in PBT for 5 minutes each. Samples were then mounted in 80% glycerol. All steps were carried out at room temperature unless otherwise stated.

Tyramide Amplification

Midguts treated with tyramide were dissected, fixed and washed as described above. The manufacturer's instructions for Alexa Fluor 488 Tyramide Superboost Kit, goat anti-mouse (Invitrogen, Cat no. B40941) was then followed. For tyramide labeling, midguts were incubated in tyramide working solution for 10 minutes.

Image Acquisition and Analysis

Images were acquired on the Zeiss LSM800 or LSM880 Confocal Microscopes as serial optical sections (z-stacks) of 1,024 x 1,024 resolution. Only the first 500μm adjacent to the pyloric ring was imaged and analysed throughout this study. This was to ensure consistent comparison of regions between midgut samples and the prevention of confounding results

due to regional midgut differences (Buchon *et al*, 2013, Marianes & Spradling, 2013). For image acquisition of tyramide treated tissues, a fixed laser intensity was used (Supplementary Table 4).

Clonal cell counts were conducted using Bitplane Imaris software to render 3D reconstructions of intestines. Imaris Spot and Surface functions were then utilized to quantify and map cell nuclei to clones.

Cell counts and fluorescent intensity measurements were performed using FIJI/ ImageJ software. FIJI was also used to process images and Adobe Photoshop used to compile figure panels. Statistical analysis and graphs were created using Graphpad PRISM.

Droplet Digital PCR

Droplet Digital PCR (ddPCR) was used to for expression analysis during this study. Taqman gene expression assays were purchased from Thermofischer Scientific (Supplementary Table 1). RNA was extracted either from 10 larval heads or at least 15 midguts per genotype using the Qiagen RNeasy Mini Kit (Cat no. 74104). RNA quality was analysed on the Agilent Tapestation 2200. RNA with an RNA Integrity Number (RIN) above 8 was used for analysis. RNA quantification was carried out on a Qubit 4 Fluorometer. 500ng of RNA was then used for cDNA synthesis using the Bioline Sensifast cDNA Synthesis Kit (Cat no. BIO-65053) as per the manufacturer's instructions.

Ackowledgements

The authors would like to thank the Bloomington *Drosophila* Stock Center, Vienna *Drosophila* RNAi Center, Kyoto *Drosophila* Stock Center, Australian *Drosophila* Biomedical Research Support Facility (OzDros), S.Hou, S. Bray, K. Harvey, L. Quinn, A. Gould, C. Samakovlis and DL. Jonesfor *Drosophila* strains; the Developmental Studies Hybridoma Bank, W. McGinnis, M.Harrison, S. Bray, and S. Thor for antibodies.

Author Contributions

ND and FC conducted all experiments. ND, NAS and GRH planned experiments. All authors were involved in writing and editing the manuscript.

Conflict of Interest

The authors have no conflicts of interest to declare.

References

Aberle H, Butz S, Stappert J, Weissig H, Kemler R, Hoschuetzky H (1994) Assembly of the cadherin-catenin complex in vitro with recombinant proteins. *J Cell Sci* 107 (Pt 12): 3655-63

Al Hayek S, Alsawadi A, Kambris Z, Boquete J-P, Bohère J, Ronsin B, Plaza S, Lemaitre B, Payre F, Osman D (2019) Shavenbaby protein isoforms orchestrate the self-renewal versus differentiation of Drosophila intestinal stem cells. 627554

Almeida MS, Bray SJ (2005) Regulation of post-embryonic neuroblasts by Drosophila Grainyhead. *Mech Dev* 122: 1282-93

Amcheslavsky A, Song W, Li Q, Nie Y, Bragatto I, Ferrandon D, Perrimon N, Ip YT (2014) Enteroendocrine cells support intestinal stem-cell-mediated homeostasis in Drosophila. *Cell Rep* 9: 32-39

Antonello ZA, Reiff T, Ballesta-Illan E, Dominguez M (2015) Robust intestinal homeostasis relies on cellular plasticity in enteroblasts mediated by miR-8-Escargot switch. *EMBO J* 34: 2025-41

Attardi LD, Tjian R (1993) Drosophila tissue-specific transcription factor NTF-1 contains a novel isoleucine-rich activation motif. *Genes Dev* 7: 1341-53

Baumgardt M, Karlsson D, Terriente J, Diaz-Benjumea FJ, Thor S (2009) Neuronal subtype specification within a lineage by opposing temporal feed-forward loops. *Cell* 139: 969-82

Bhandari A, Gordon W, Dizon D, Hopkin AS, Gordon E, Yu Z, Andersen B (2013) The Grainyhead transcription factor Grhl3/Get1 suppresses miR-21 expression and tumorigenesis in skin: modulation of the miR-21 target MSH2 by RNA-binding protein DND1. *Oncogene* 32: 1497-507

Biteau B, Hochmuth CE, Jasper H (2008) JNK activity in somatic stem cells causes loss of tissue homeostasis in the aging Drosophila gut. *Cell Stem Cell* 3: 442-55

Biteau B, Jasper H (2014) Slit/Robo signaling regulates cell fate decisions in the intestinal stem cell lineage of Drosophila. *Cell Rep* 7: 1867-75

Blastyak A, Mishra RK, Karch F, Gyurkovics H (2006) Efficient and specific targeting of Polycomb group proteins requires cooperative interaction between Grainyhead and Pleiohomeotic. *Mol Cell Biol* 26: 1434-44

Bohere J, Mancheno-Ferris A, Al Hayek S, Zanet J, Valenti P, Akino K, Yamabe Y, Inagaki S, Chanut-Delalande H, Plaza S, Kageyama Y, Osman D, Polesello C, Payre F (2018) Shavenbaby and Yorkie mediate Hippo signaling to protect adult stem cells from apoptosis. *Nat Commun* 9: 5123

Bray SJ, Burke B, Brown NH, Hirsh J (1989) Embryonic expression pattern of a family of Drosophila proteins that interact with a central nervous system regulatory element. *Genes Dev* 3: 1130-45

Bray SJ, Kafatos FC (1991) Developmental function of Elf-1: an essential transcription factor during embryogenesis in Drosophila. *Genes Dev* 5: 1672-83

Buchon N, Broderick NA, Kuraishi T, Lemaitre B (2010) Drosophila EGFR pathway coordinates stem cell proliferation and gut remodeling following infection. *BMC Biol* 8: 152

Buchon N, Osman D, David FP, Fang HY, Boquete JP, Deplancke B, Lemaitre B (2013) Morphological and molecular characterization of adult midgut compartmentalization in Drosophila. *Cell Rep* 3: 1725-38

Cenci C, Gould AP (2005) Drosophila Grainyhead specifies late programmes of neural proliferation by regulating the mitotic activity and Hox-dependent apoptosis of neuroblasts. *Development* 132: 3835-45

Chen J, Xu N, Wang C, Huang P, Huang H, Jin Z, Yu Z, Cai T, Jiao R, Xi R (2018) Transient Scute activation via a self-stimulatory loop directs enteroendocrine cell pair specification from self-renewing intestinal stem cells. *Nat Cell Biol* 20: 152-161

Chen W, Xiao Liu Z, Oh JE, Shin KH, Kim RH, Jiang M, Park NH, Kang MK (2012) Grainyhead-like 2 (GRHL2) inhibits keratinocyte differentiation through epigenetic mechanism. *Cell Death Dis* 3: e450

Chung VY, Tan TZ, Tan M, Wong MK, Kuay KT, Yang Z, Ye J, Muller J, Koh CM, Guccione E, Thiery JP, Huang RY (2016) GRHL2-miR-200-ZEB1 maintains the epithelial status of ovarian cancer through transcriptional regulation and histone modification. *Sci Rep* 6: 19943

Cieply B, Farris J, Denvir J, Ford HL, Frisch SM (2013) Epithelial-mesenchymal transition and tumor suppression are controlled by a reciprocal feedback loop between ZEB1 and Grainyhead-like-2. *Cancer Res* 73: 6299-309

Cieply B, Riley Pt, Pifer PM, Widmeyer J, Addison JB, Ivanov AV, Denvir J, Frisch SM (2012) Suppression of the epithelial-mesenchymal transition by Grainyhead-like-2. *Cancer Res* 72: 2440-53

Clark RI, Salazar A, Yamada R, Fitz-Gibbon S, Morselli M, Alcaraz J, Rana A, Rera M, Pellegrini M, Ja WW, Walker DW (2015) Distinct Shifts in Microbiota Composition during Drosophila Aging Impair Intestinal Function and Drive Mortality. *Cell Rep* 12: 1656-67

Dantoft W, Davis MM, Lindvall JM, Tang X, Uvell H, Junell A, Beskow A, Engstrom Y (2013) The Oct1 homolog Nubbin is a repressor of NF-kappaB-dependent immune gene expression that increases the tolerance to gut microbiota. *BMC Biol* 11: 99

Dantoft W, Lundin D, Esfahani SS, Engstrom Y (2016) The POU/Oct Transcription Factor Pdm1/nub Is Necessary for a Beneficial Gut Microbiota and Normal Lifespan of Drosophila. *J Innate Immun* 8: 412-26

Dutta D, Dobson AJ, Houtz PL, Glasser C, Revah J, Korzelius J, Patel PH, Edgar BA, Buchon N (2015) Regional Cell-Specific Transcriptome Mapping Reveals Regulatory Complexity in the Adult Drosophila Midgut. *Cell Rep* 12: 346-58

Dynlacht BD, Attardi LD, Admon A, Freeman M, Tjian R (1989) Functional analysis of NTF-1, a developmentally regulated Drosophila transcription factor that binds neuronal cis elements. *Genes Dev* 3: 1677-88

Fan Y, Bergmann A (2010) The cleaved-Caspase-3 antibody is a marker of Caspase-9-like DRONC activity in Drosophila. *Cell Death Differ* 17: 534-9

Fogarty CE, Bergmann A (2014) Detecting caspase activity in Drosophila larval imaginal discs. *Methods Mol Biol* 1133: 109-17

Gao X, Vockley CM, Pauli F, Newberry KM, Xue Y, Randell SH, Reddy TE, Hogan BL (2013) Evidence for multiple roles for grainyhead-like 2 in the establishment and maintenance of human mucociliary airway epithelium. *Proc Natl Acad Sci U S A* 110: 9356-61

Gregory PA, Bert AG, Paterson EL, Barry SC, Tsykin A, Farshid G, Vadas MA, Khew-Goodall Y, Goodall GJ (2008) The miR-200 family and miR-205 regulate epithelial to mesenchymal transition by targeting ZEB1 and SIP1. *Nat Cell Biol* 10: 593-601

Grob TJ, Novak U, Maisse C, Barcaroli D, Luthi AU, Pirnia F, Hugli B, Graber HU, De Laurenzi V, Fey MF, Melino G, Tobler A (2001) Human delta Np73 regulates a dominant negative feedback loop for TAp73 and p53. *Cell Death Differ* 8: 1213-23

Guo Z, Driver I, Ohlstein B (2013) Injury-induced BMP signaling negatively regulates Drosophila midgut homeostasis. *J Cell Biol* 201: 945-61

Harrison MM, Botchan MR, Cline TW (2010) Grainyhead and Zelda compete for binding to the promoters of the earliest-expressed Drosophila genes. *Dev Biol* 345: 248-55

Hay BA, Wolff T, Rubin GM (1994) Expression of baculovirus P35 prevents cell death in Drosophila. *Development* 120: 2121-9

Hindson BJ, Ness KD, Masquelier DA, Belgrader P, Heredia NJ, Makarewicz AJ, Bright IJ, Lucero MY, Hiddessen AL, Legler TC, Kitano TK, Hodel MR, Petersen JF, Wyatt PW, Steenblock ER, Shah PH, Bousse LJ, Troup CB, Mellen JC, Wittmann DK et al. (2011) High-throughput droplet digital PCR system for absolute quantitation of DNA copy number. *Anal Chem* 83: 8604-10

Horvay K, Casagranda F, Gany A, Hime GR, Abud HE (2011) Wnt signaling regulates Snai1 expression and cellular localization in the mouse intestinal epithelial stem cell niche. *Stem Cells Dev* 20: 737-45

Horvay K, Jarde T, Casagranda F, Perreau VM, Haigh K, Nefzger CM, Akhtar R, Gridley T, Berx G, Haigh JJ, Barker N, Polo JM, Hime GR, Abud HE (2015) Snai1 regulates cell lineage allocation and stem cell maintenance in the mouse intestinal epithelium. *Embo j* 34: 1319-35

Huang JD, Dubnicoff T, Liaw GJ, Bai Y, Valentine SA, Shirokawa JM, Lengyel JA, Courey AJ (1995) Binding sites for transcription factor NTF-1/Elf-1 contribute to the ventral repression of decapentaplegic. *Genes Dev* 9: 3177-89

Hudry B, Khadayate S, Miguel-Aliaga I (2016) The sexual identity of adult intestinal stem cells controls organ size and plasticity. *Nature* 530: 344-8

Hung RJ, Hu Y, Kirchner R, Liu Y, Xu C, Comjean A, Tattikota SG, Li F, Song W, Ho Sui S, Perrimon N (2020) A cell atlas of the adult Drosophila midgut. *Proc Natl Acad Sci U S A* 117: 1514-1523

Jacobs J, Atkins M, Davie K, Imrichova H, Romanelli L, Christiaens V, Hulselmans G, Potier D, Wouters J, Taskiran, II, Paciello G, Gonzalez-Blas CB, Koldere D, Aibar S, Halder G, Aerts S (2018) The transcription factor Grainy head primes epithelial enhancers for spatiotemporal activation by displacing nucleosomes. *Nat Genet* 50: 1011-1020

Jiang H, Patel PH, Kohlmaier A, Grenley MO, McEwen DG, Edgar BA (2009) Cytokine/Jak/Stat signaling mediates regeneration and homeostasis in the Drosophila midgut. *Cell* 137: 1343-55

Kim M, McGinnis W (2011) Phosphorylation of Grainy head by ERK is essential for wound-dependent regeneration but not for development of an epidermal barrier. *Proc Natl Acad Sci U S A* 108: 650-5

Klapper R (2000) The longitudinal visceral musculature of Drosophila melanogaster persists through metamorphosis. *Mech Dev* 95: 47-54

Kondo T, Plaza S, Zanet J, Benrabah E, Valenti P, Hashimoto Y, Kobayashi S, Payre F, Kageyama Y (2010) Small peptides switch the transcriptional activity of Shavenbaby during Drosophila embryogenesis. *Science* 329: 336-9

Korzelius J, Naumann SK, Loza-Coll MA, Chan JS, Dutta D, Oberheim J, Glasser C, Southall TD, Brand AH, Jones DL, Edgar BA (2014) Escargot maintains stemness and suppresses differentiation in Drosophila intestinal stem cells. *EMBO J* 33: 2967-82

LaJeunesse DR, Johnson B, Presnell JS, Catignas KK, Zapotoczny G (2010) Peristalsis in the junction region of the Drosophila larval midgut is modulated by DH31 expressing enteroendocrine cells. *BMC Physiol* 10: 14

Lee T, Luo L (1999) Mosaic analysis with a repressible cell marker for studies of gene function in neuronal morphogenesis. *Neuron* 22: 451-61

Lee WC, Beebe K, Sudmeier L, Micchelli CA (2009) Adenomatous polyposis coli regulates Drosophila intestinal stem cell proliferation. *Development* 136: 2255-64

Liang J, Balachandra S, Ngo S, O'Brien LE (2017) Feedback regulation of steady-state epithelial turnover and organ size. *Nature* 548: 588-591

Liaw GJ, Rudolph KM, Huang JD, Dubnicoff T, Courey AJ, Lengyel JA (1995) The torso response element binds GAGA and NTF-1/Elf-1, and regulates tailless by relief of repression. *Genes Dev* 9: 3163-76

Lin G, Xu N, Xi R (2008) Paracrine Wingless signalling controls self-renewal of Drosophila intestinal stem cells. *Nature* 455: 1119-23

Lin G, Xu N, Xi R (2010) Paracrine unpaired signaling through the JAK/STAT pathway controls self-renewal and lineage differentiation of drosophila intestinal stem cells. *J Mol Cell Biol* 2: 37-49

Lindberg BG, Tang X, Dantoft W, Gohel P, Seyedoleslami Esfahani S, Lindvall JM, Engstrom Y (2018) Nubbin isoform antagonism governs Drosophila intestinal immune homeostasis. *PLoS Pathog* 14: e1006936

Linneweber GA, Jacobson J, Busch KE, Hudry B, Christov CP, Dormann D, Yuan M, Otani T, Knust E, de Bono M, Miguel-Aliaga I (2014) Neuronal control of metabolism through nutrient-dependent modulation of tracheal branching. *Cell* 156: 69-83

Loza-Coll MA, Southall TD, Sandall SL, Brand AH, Jones DL (2014) Regulation of Drosophila intestinal stem cell maintenance and differentiation by the transcription factor Escargot. *EMBO J* 33: 2983-96

Mace KA, Pearson JC, McGinnis W (2005) An epidermal barrier wound repair pathway in Drosophila is mediated by grainy head. *Science* 308: 381-5

Mani SA, Guo W, Liao MJ, Eaton EN, Ayyanan A, Zhou AY, Brooks M, Reinhard F, Zhang CC, Shipitsin M, Campbell LL, Polyak K, Brisken C, Yang J, Weinberg RA (2008) The epithelial-mesenchymal transition generates cells with properties of stem cells. *Cell* 133: 704-15

Marianes A, Spradling AC (2013) Physiological and stem cell compartmentalization within the Drosophila midgut. *Elife* 2: e00886

Micchelli CA, Perrimon N (2006) Evidence that stem cells reside in the adult Drosophila midgut epithelium. *Nature* 439: 475-9

Miles LB, Dworkin S, Darido C (2017) Alternative splicing and start sites: Lessons from the Grainyhead-like family. *Dev Biol* 429: 12-19

Mlacki M, Darido C, Jane SM, Wilanowski T (2014) Loss of Grainy head-like 1 is associated with disruption of the epidermal barrier and squamous cell carcinoma of the skin. *PLoS One* 9: e89247

Muller M, Schilling T, Sayan AE, Kairat A, Lorenz K, Schulze-Bergkamen H, Oren M, Koch A, Tannapfel A, Stremmel W, Melino G, Krammer PH (2005) TAp73/Delta Np73 influences apoptotic response, chemosensitivity and prognosis in hepatocellular carcinoma. *Cell Death Differ* 12: 1564-77

Murray-Zmijewski F, Lane DP, Bourdon JC (2006) p53/p63/p73 isoforms: an orchestra of isoforms to harmonise cell differentiation and response to stress. *Cell Death Differ* 13: 962-72

Narasimha M, Uv A, Krejci A, Brown NH, Bray SJ (2008) Grainy head promotes expression of septate junction proteins and influences epithelial morphogenesis. *J Cell Sci* 121: 747-52

Nevil M, Bondra ER, Schulz KN, Kaplan T, Harrison MM (2017) Stable Binding of the Conserved Transcription Factor Grainy Head to its Target Genes Throughout Drosophila melanogaster Development. *Genetics* 205: 605-620

Nevil M, Gibson TJ, Bartolutti C, Iyengar A, Harrison MM (2020) Establishment of chromatin accessibility by the conserved transcription factor Grainy head is developmentally regulated. *Development* 147

Ni JQ, Zhou R, Czech B, Liu LP, Holderbaum L, Yang-Zhou D, Shim HS, Tao R, Handler D, Karpowicz P, Binari R, Booker M, Brennecke J, Perkins LA, Hannon GJ, Perrimon N (2011) A genome-scale shRNA resource for transgenic RNAi in Drosophila. *Nat Methods* 8: 405-7

Niwa H, Miyazaki J, Smith AG (2000) Quantitative expression of Oct-3/4 defines differentiation, dedifferentiation or self-renewal of ES cells. *Nat Genet* 24: 372-6

Nüsslein Volhard C, Nsslein-Volhard C, Wieschaus E, Kluding H (1984) Mutations affecting the pattern of the larval cuticle inDrosophila melanogaster. *Wilhelm Roux's archives of developmental biology* 193: 267-282

Ohlstein B, Spradling A (2006) The adult Drosophila posterior midgut is maintained by pluripotent stem cells. *Nature* 439: 470-4

Ohlstein B, Spradling A (2007) Multipotent Drosophila intestinal stem cells specify daughter cell fates by differential notch signaling. *Science* 315: 988-92

Pfeiffer BD, Jenett A, Hammonds AS, Ngo TT, Misra S, Murphy C, Scully A, Carlson JW, Wan KH, Laverty TR, Mungall C, Svirskas R, Kadonaga JT, Doe CQ, Eisen MB, Celniker SE, Rubin GM

(2008) Tools for neuroanatomy and neurogenetics in Drosophila. *Proc Natl Acad Sci U S A* 105: 9715-20

Quan Y, Jin R, Huang A, Zhao H, Feng B, Zang L, Zheng M (2014) Downregulation of GRHL2 inhibits the proliferation of colorectal cancer cells by targeting ZEB1. *Cancer Biol Ther* 15: 878-87

Quan Y, Xu M, Cui P, Ye M, Zhuang B, Min Z (2015) Grainyhead-like 2 Promotes Tumor Growth and is Associated with Poor Prognosis in Colorectal Cancer. *J Cancer* 6: 342-50

Rera M, Clark RI, Walker DW (2012) Intestinal barrier dysfunction links metabolic and inflammatory markers of aging to death in Drosophila. *Proc Natl Acad Sci U S A* 109: 21528-33

Scopelliti A, Cordero JB, Diao F, Strathdee K, White BH, Sansom OJ, Vidal M (2014) Local control of intestinal stem cell homeostasis by enteroendocrine cells in the adult Drosophila midgut. *Curr Biol* 24: 1199-211

Tai K, Cockburn K, Greco V (2019) Flexibility sustains epithelial tissue homeostasis. *Curr Opin Cell Biol* 60: 84-91

Tang X, Zhao Y, Buchon N, Engstrom Y (2018) The POU/Oct Transcription Factor Nubbin Controls the Balance of Intestinal Stem Cell Maintenance and Differentiation by Isoform-Specific Regulation. *Stem Cell Reports* 10: 1565-1578

Tanimizu N, Kobayashi S, Ichinohe N, Mitaka T (2014) Downregulation of miR122 by grainyhead-like 2 restricts the hepatocytic differentiation potential of adult liver progenitor cells. *Development* 141: 4448-56

Tanimizu N, Nakamura Y, Ichinohe N, Mizuguchi T, Hirata K, Mitaka T (2013) Hepatic biliary epithelial cells acquire epithelial integrity but lose plasticity to differentiate into hepatocytes in vitro during development. *J Cell Sci* 126: 5239-46

Ting SB, Wilanowski T, Cerruti L, Zhao LL, Cunningham JM, Jane SM (2003) The identification and characterization of human Sister-of-Mammalian Grainyhead (SOM) expands the grainyhead-like family of developmental transcription factors. *Biochem J* 370: 953-62

Tomasini R, Tsuchihara K, Wilhelm M, Fujitani M, Rufini A, Cheung CC, Khan F, Itie-Youten A, Wakeham A, Tsao MS, Iovanna JL, Squire J, Jurisica I, Kaplan D, Melino G, Jurisicova A, Mak TW (2008) TAp73 knockout shows genomic instability with infertility and tumor suppressor functions. *Genes Dev* 22: 2677-91

Traylor-Knowles N, Hansen U, Dubuc TQ, Martindale MQ, Kaufman L, Finnerty JR (2010) The evolutionary diversification of LSF and Grainyhead transcription factors preceded the radiation of basal animal lineages. *BMC Evolutionary Biology* 10: 101

Tuckfield A, Clouston DR, Wilanowski TM, Zhao LL, Cunningham JM, Jane SM (2002) Binding of the RING polycomb proteins to specific target genes in complex with the grainyhead-like family of developmental transcription factors. *Mol Cell Biol* 22: 1936-46

Uv AE, Harrison EJ, Bray SJ (1997) Tissue-specific splicing and functions of the Drosophila transcription factor Grainyhead. *Mol Cell Biol* 17: 6727-35

Venkatesan K, McManus HR, Mello CC, Smith TF, Hansen U (2003) Functional conservation between members of an ancient duplicated transcription factor family, LSF/Grainyhead. *Nucleic Acids Res* 31: 4304-16

Vert JP, Foveau N, Lajaunie C, Vandenbrouck Y (2006) An accurate and interpretable model for siRNA efficacy prediction. *BMC Bioinformatics* 7: 520

Wang J, Liu YX, Hande MP, Wong AC, Jin YJ, Yin Y (2007) TAp73 is a downstream target of p53 in controlling the cellular defense against stress. *J Biol Chem* 282: 29152-62

Wang S, Samakovlis C (2012) Grainy head and its target genes in epithelial morphogenesis and wound healing. *Curr Top Dev Biol* 98: 35-63

Wang S, Tsarouhas V, Xylourgidis N, Sabri N, Tiklova K, Nautiyal N, Gallio M, Samakovlis C (2009) The tyrosine kinase Stitcher activates Grainy head and epidermal wound healing in Drosophila. *Nat Cell Biol* 11: 890-5

Werner S, Frey S, Riethdorf S, Schulze C, Alawi M, Kling L, Vafaizadeh V, Sauter G, Terracciano L, Schumacher U, Pantel K, Assmann V (2013) Dual roles of the transcription factor grainyhead-like 2 (GRHL2) in breast cancer. *J Biol Chem* 288: 22993-3008

Wilanowski T, Tuckfield A, Cerruti L, O'Connell S, Saint R, Parekh V, Tao J, Cunningham JM, Jane SM (2002) A highly conserved novel family of mammalian developmental transcription factors related to Drosophila grainyhead. *Mech Dev* 114: 37-50

Yu Z, Mannik J, Soto A, Lin KK, Andersen B (2009) The epidermal differentiation-associated Grainyhead gene Get1/Grhl3 also regulates urothelial differentiation. *EMBO J* 28: 1890-903

Zanet J, Benrabah E, Li T, Pelissier-Monier A, Chanut-Delalande H, Ronsin B, Bellen HJ, Payre F, Plaza S (2015) Pri sORF peptides induce selective proteasome-mediated protein processing. *Science* 349: 1356-8

Zeng X, Han L, Singh SR, Liu H, Neumuller RA, Yan D, Hu Y, Liu Y, Liu W, Lin X, Hou SX (2015) Genome-wide RNAi screen identifies networks involved in intestinal stem cell regulation in Drosophila. *Cell Rep* 10: 1226-38

Zeng X, Hou SX (2015) Enteroendocrine cells are generated from stem cells through a distinct progenitor in the adult Drosophila posterior midgut. *Development* 142: 644-53

Zheng H, Kang Y (2014) Multilayer control of the EMT master regulators. *Oncogene* 33: 1755-63

Zhou J, Florescu S, Boettcher AL, Luo L, Dutta D, Kerr G, Cai Y, Edgar BA, Boutros M (2015) Dpp/Gbb signaling is required for normal intestinal regeneration during infection. *Dev Biol* 399: 189-203

Figure Legends

Figure 1. *grh* is expressed in the midgut.

A) Schematic of *grh* mRNA transcripts. The single *grh* gene is alternatively spliced to produce 8 mRNA transcripts. These transcripts are classed into two groups based on the splicing of exons 4 and 5 (red box). Transcripts with exons 4 and 5 are classed as O-isoforms while those without these exons are classed as N-isoforms.

B) Quantification of *esg*, *sna* and *grh* mRNA transcripts in 5-7-day old adult w^{1118} midguts shows that in comparison to known ISC/EB marker *esg*, *grh* transcripts are expressed at much lower levels but is more comparable to that of ISC regulator, *sna.* mRNA quantification was conducted using biological triplicates (n=15 midguts for each replicate) with each replicate represented by individual data points. Bar graph represents mean ± SEM of data points.

C-D) Tyramide treated midguts of *GMR41CO9-Gal4 > UAS-GFP and* w^{1118} fly strains. An amplified GFP signal can be detected in cells with small nuclei (inset) in *GMR41CO9-Gal4 > UAS-GFP* **(C)** but not in w^{1118} **(D)** negative controls. Scale Bar 40µm.

E-F) Midguts of *GMR44G11-Gal4 > UAS-GFP* and w^{1118} strains treated with tyramide. A tyramide amplified GFP signal was observed in cells with small nuclei (inset) in *GMR44G11-Gal4 > UAS-GFP* **(E)** but not in concurrently treated w^{1118} midguts **(F)**. Scale Bar 40µm.

Figure 2. *grh* O-isoforms maintain ISC identity

A-H) Representative maximal intensity z-projections of GFP (green) marked control, grh^{S2140}, grh^{IM} *and* grh^{370} MARCM clones at 5PDCI and 10DPCI. Scale Bar 40µm.

I) Quantification of the mean number of clones per midgut over time. MARCM control (5DPCI: n=18 midguts, 10DPCI n=26 midguts) and *grh* null (grh^{S2140} – 5DPCI: n=7 midguts, 10DPCI n= 23 midguts; grh^{IM} – 5DPCI: n=6 midguts 10DPCI: n=28 midguts) clones increase over time while O-specific mutant grh^{370} (5DPCI: n= 10 midguts, 10DPCI: n= 25 midguts) clones are lost. (Mean ± SEM, Two-way ANOVA with Tukey's test, ns= not significant, ****p<0.0001).

J) Proportion of MARCM clones at 10DPCI containing at least a single Dl+ ISC in control (n=14), *grh*^{S2140} (n=8), *grh*^{IM} (n=14) and *grh*^{370} (n=18) midguts. In comparison to control clones, there is a significant decrease in the fraction of *grh*^{370} clones containing ISCs. (Mean ± SEM, One-Way ANOVA with Tukey's test, ns= not significant, ****p<0.0001).

K-L) Confocal images of control and *esg*^{TS}*> UAS-grh.O RNAi* midguts. ISCs are marked by Dl and progenitor cells marked with GFP. Scale Bar 40µm.

M) Quantification of Dl+ ISC cells in control (n=22 midguts) and *esg*^{TS}*> UAS-grh.O RNAi* (n=24 midguts) midguts showed a decrease in the proportion of Dl+ cells over total cell number. (Mean ± SEM, Unpaired students T-test with Welsh's Correction, **p=0.0078).

N) Proportion of esg+ cells that are Dl+ ISCs in control (n=22 midguts) and *esg*^{TS}*> UAS-grh.O RNAi* (n=24 midguts). (Mean ± SEM, Unpaired students T-test with Welsh's Correction, **p=0.0049).

O) Quantification of the proportion of Dl+ ISCs over total cell number in control (n=12 midguts) and *esg*^{TS}*>UAS-grh.ALL RNAi* (n=18 midguts) show no significant difference between the two genotypes. (Mean ± SEM, Unpaired students T-test with Welsh's Correction, ns = not significant).

P) The proportion of esg+ cells that are Dl+ ISCs remain at similar levels in control (n=12 midguts) and *esg*^{TS}*> UAS-grh.ALL RNAi* (n=18 midguts) midguts. (Mean ± SEM, Unpaired students T-test with Welsh's Correction, ns = not significant).

Figure 3. Ectopic expression of the N-isoform, grh.RP promotes differentiation

A-D) Representative images of control midguts **(A)**, midguts over expressing grh.RP **(B)**, the apoptotic inhibitor p35 **(C)** and midguts co-expressing p35 and grh.RP **(D)** in progenitor cells. Scale Bar 40µm.

E) Quantification of the number of progenitor cells in control (n=15 midguts) midguts, midguts over expressing grh.RP (n=19 midguts), p35 (n=22 midguts) and midguts co-expressing grh.RP

and p35 (n=7 midguts) shows that expression of p35 was not able to rescue loss of progenitor cells. (Mean ± SEM, One-Way ANOVA with Tukey's Test, ns= not significant, ****p<0.0001).

F) Quantification of the proportion of ISC/EBs in control and *esg^{TS}> UAS-grh.RH* midguts. The proportion of progenitors in *esg^{TS}> UAS-grh.RH* midguts (n=21) have decreased in comparison to control midguts (n=13). (Mean ± SEM, Unpaired students T-test, **p=0.0088).

G-J) Confocal images of control **(G)** and midguts ectopically expressing N-isoform, grh.RP **(H)** and grh. RH **(I)** and O-isoform, grh.RL **(J)** in ISC/EBs. Compared to controls, GFP+ progenitor cells expressing grh.RP, grh.RH or grh.RL have increased cell size and also express the EC marker, Pdm-1 (arrows). Scale Bar 40μm.

K) The proportion of esg+ progenitor cells expressing Pdm-1 in midguts increases in midguts over expressing grh.RP (n=15) and grh.RL (n=9) in comparison to control midguts (n=11). While the proportion of esg+ progenitor cells expressing Pdm-1 slightly increased in midguts overexpressing grh.RH (n=19), it was not statistically significant compared to controls. (Mean ± SEM, One-Way ANOVA with Tukey's Test, ns=not significant, *p=0.0107, ****p<0.0001).

Figure 4. Over expression of O-isoform, grh.RL results in both ISC maintenance and differentiation

A-B) Control midguts and midguts over expressing the O-isoform, grh.RL in progenitor cells. While only some progenitor cells express ISC marker, Dl **(A)** a majority of *esg^{TS} > UAS-grh.RL* cells express Dl **(B)**.

C) In comparison to control midguts (n=13) there is an increase in the proportion of esg+ cells in midguts over expressing grh.RL (n=13). (Mean ± SEM, Unpaired students T-test with Welsh's Correction, ****p<0.0001).

D) An increase in the mitotic index as measured by the number of pH3+ cells are observed in midguts ectopically expressing grh.RL (n= 16). This increase in mitotic index is rescued by the co-expression of the apoptotic inhibitor p35 with grh.RL (n= 9) with its mitotic index returning to levels seen in control midguts (n= 16) and midguts only expressing p35 (n= 6). (Mean ± SEM, One-Way ANOVA with Tukey's Test, **p=0.0027, ***p=0.0001, ****p<0.0001).

E-F) Confocal images of control midguts and midguts ectopically expressing grh.RL in only ISCs (green). Ectopically expressing grh.RL in ISCs does not appear induce differentiation with the YFP+ ISCs remaining at a similar size to YFP+ cells in control midguts. Scale Bar 40μm.

G) The proportion of ISCs in control midguts (n=20) and midguts ectopically expressing grh.RL (n=17) remain at similar level. (Mean ± SEM, Unpaired students T-test with Welsh's Correction, p=0.0749).

H) In comparison to controls (n=11 midguts), an increase in GFP+ EBs is observed in midguts ectopically expressing grh.RL (n=4). (Mean ± SEM, Unpaired students T-test with Welsh's Correction, ****p<0.0001).

I-J) Representative images of control midguts **(I)** and midguts over expressing grh.RL **(J)** in EBs. In control midguts, ISCs are solely marked by Dl with mitotically active ISCs marked by pH3 (arrowheads) whereas over expression of grh.RL in EBs induces EB expression of Dl and EB mitotic division (arrows). Scale Bar 40μm.

K) Comparison of the mitotic index in control midguts (n=19) and midguts over expressing grh.RL (n=14) in EBs. An increase in the mitotic index is observed in midguts over expressing grh.RL in EBs. (Mean ± SEM, Unpaired students T-test, ****p<0.0001).

L) Quantification of the number of EBs undergoing mitotic division. (Mean ± SEM, Unpaired students T-test, ****p<0.0001).

M-N) Confocal images of control midguts and midguts over expressing grh.RL in EBs immunostained with EC marker, Pdm-1. Whereas GFP+ EBs in controls rarely express Pdm-1, an increase in *Su(H)^{TS} > UAS-grh.RL* cells are positive for Pdm-1 is observed. Scale Bar 40μm.

O) The proportion of EBs expressing Pdm-1 increases in *Su(H)^{TS} > UAS-grh.RL* midguts (n=4) in comparison to control midguts (n= 11). (Mean ± SEM, Unpaired students T-test, ****p<0.0001).

Figure 5. grh.RL interacts with zfh-1 and *miR-8*

A-F) Representative images of control midguts **(A)**, midguts ectopically expressing grh.RL **(B)**, a *miR-8* sponge **(C)**, zfh-1 **(D)** and midguts co-expressing grh.RL and the miR-8 sponge **(E)** or zfh-1 **(F)**. Scale Bar 40μm.

G) Quantification of the proportion of ISC/EBs over total cells for each genotype used in this experiment. (Control: n=24, grh.RL n=13, miR-8 sponge n=18, zfh-1 n=21, miR-8 sponge + grh.RL n=9, zfh-1 + grh.RL n=14 midguts) (Mean ± SEM, One-Way ANOVA with Tukey's Test, ****p<0.0001).

H) Quantification of the nuclear size of ISC/EBs for each genotype used in this experiment. (Control: n=24, grh.RL n=13, miR-8 sponge n=18, zfh-1 n=21, miR-8 sponge + grh.RL n=9, zfh-1 + grh.RL n=14 midguts) (Mean ± SEM, One-Way ANOVA with Tukey's Test, **p=0.0047, ****p<0.0001).

I) Proposed model of Grh.RL interaction with *miR-8* and Zfh-1. In this small network, Grh.RL is able to activate *miR-8* to induce EB differentiation to ECs as seen by the enlarged nuclear size in *esg*^{TS} > *UAS-grh.RL* midguts that is rescued upon co-expression of *a miR-8* sponge. This interaction is potentially regulated by Zfh-1 inhibition of Grh.RL as the enlarged nuclear size observed in *esg*^{TS} > *UAS-grh.RL* midguts is also rescued by the co-expression of Zfh-1 and Grh.RL.

Tables (Supplementary):

Supplementary Table 1: TaqMan Gene Expression Assays

Gene Name	**Assay ID**
sna	Dm01841564_s1
esg	Dm01841264_s1
grh-RK	Dm01816384_m1
grh-ALL	Dm01816396_m1
grh-RL, RJ, RN, RO	Dm01816390_g1
grh-RL, RJ	Dm01841950_m1
RpL32	Dm02151827_g1
RpL11	Dm01842483_g1

Supplementary Table 2: *grh-Gal4* lines tested

grh-Gal4* Line > *10xUAS-IVS-myr::GFP	**- Tyramide**	**+ Tyramide**
BDSC_76172 *grh[MI05134-TG4.O]/SM6a*	-	-
BDSC_65637 *grh[1249-G4]*	-	-
BDSC_64345 *GMR43D01-Gal4*	-	-
BDSC_49387 *GMR41C09-Gal4*	-	+
BDSC_45301 *GMR43CO2-Gal4*	-	-
BDSC_46228 *GMR40A02-Gal4*	-	-
BDSC_47932 *GMR44G11-Gal4*	-	+
BDSC_45299 *GMR43B01-Gal4*	-	-
BDSC_45275 *GMR41A10-Gal4*	-	-
BDSC_45685 *GMR40G05-Gal4*	-	-
BDSC_47589 *GMR42E09-Gal4*	-	-

Supplementary Table 3: Fly Strains Used in this Study

Fly Strain	**Source**
w^{1118}	Bloomington Drosophila Stock Centre BDSC_3605
grh^{S2140}/CyO	BDSC_10460
Su(H)GBE-Gal4, UAS-GFP / CyO	Stephen Hou
Delta-LacZ	BDSC_11651
GBE[1]-LacZ	Sarah Bray
GBE[2]-LacZ	Sarah Bray
grh^{06850}/CyO	BDSC_12325
grh-GFP (w[1118]; PBac {y[+mDint2] w[+mC]=grh-GFP.FPTB})VK00033)	BDSC_42272
esg^{TS} (esgGal4, UAS GFP; $TubGal80^{TS}$/ [SM6B-TM6B])	Kieran Harvey
MARCM42D (hs-FLP, UAS-CD8GFP; FRT42DtubGal80/ CyO; Tub-Gal4/TM6B)	Leonie Quinn
b pr cn grh^{370}bw/CyO	Alex Gould
cn^{1} grh^{IM} bw^{1}/ SM6a	BDSC_3270
UAS-grh.RL	BDSC_42227/42228
UAS-grh.RP/I	Christos Samakovlis
esg;Su(H)::Gal80 (w; esg-Gal4, UAS-2xYFP/ CyO; Su(H)Gal80, $TubGal80^{TS}$/ TM3)	Leanne Jones
UAS-grh.RH	This Study
UAS-Zfh-1	BDSC_6879

w; UAS-mCherry-mir-8-sponge/ CyO; UAS-mCherry-mir-8-sponge*	BDSC_61374
UAS-10x-UAS-IVS-myr-GFP	BDSC_32197
UAS-grh.O RNAi	This Study
UAS-P35	BDSC_5073
grh^{WG}/ CyO	This Study

Supplementary Table 4: Microscope Settings

Figure	Time and Space Resolution (XYZT)	Pixel Resolution	Bit Depth	Objective	Zoom	Laser Power
1C and 1D	T: 1 X: 1024 Z: 1024 Z: 21/ 20	1024 x 1024	8-bit	Plan-Apochromat 20x/ 0.8 M27	1.7x	Alexa Fluor 488 – Argon Remote Laser – Laser 0.02% DAPI – Diode 405-30 Laser – Laser Power 0.03%
1E and 1F	T: 1 X: 1024 Y: 1024 Z: 15/ 20	1024 x 1024	8-bit	Plan-Apochromat 20x/ 0.8 M27	1.7x	Alexa Fluor 488 – Argon Remote Laser – Laser Power 0.02% DAPI – Diode 405-30 Laser – Laser Power 0.03%
Supplementary Figure 2A-D	T: 1 X: 1024 Y: 1024 Z: 12/9/7/15	1024 x 1024	8-bit	Plan-Apochromat 40x/ 1.3 Oil DIC UV-IR M27	0.8x	Alexa Fluor 488 – Argon Remote Laser – Laser Power 0.02% DAPI – Diode 405-30 Laser – Laser Power 0.03%

Supplementary Figure Legends

Supplementary Figure 1. Grh expression could not be discerned using antibodies and reporter lines

(A-D) Adult midguts immunostained with four different Grh antibodies. Grh staining was not observed in phenotypically wild type midguts. ISCs were labelled by the reporter *Dl-LacZ* while *Su(H)GBE-Gal4>UAS-GFP* was used to mark EBs. Scale Bar 40μm.

(E-F) A fifth Grh antibody detects a cytoplasmic Grh (red) signal in the midgut that co-localizes with Prospero positive EE cells (magenta). However, this signal is not specific to Grh in the midgut as it can be detected in both control and homozygous *grh* null mutant MARCM clones (green). Scale Bar 40μm.

(G-H) Representative midgut z-projection images of transgenic lines carrying P-element enhancer traps within the *grh* gene. A β-galactosidase (green) signal was not observed in grh^{S2140}*-LacZ* **(G)** or grh^{06850}*-LacZ* **(H)** midguts. Scale Bar 40μm.

(I-J) Transgenic lines carrying Grh binding element fused to *LacZ* gene reporting on Grh activity. A ß-galactosidase (green) signal could not detected in midguts of *GBE-LacZ* (reports on all GRH isoforms) **(I)** or in midguts of *GBE[2]-LacZ* **(J)**, a reporter specific to the CNS Grh isoform. Scale Bar 40μm.

(K) Midgut of GFP tagged Grh transgenic line (*grh-GFP)* immunostained with an anti-GFP antibody. GFP (green) staining was undetectable. Scale Bar 40μm.

Supplementary Figure 2. Tyramide Amplification in larval third instar eye discs

(A-B) Representative images of tyramide treated **(A)** and non-tyramide treated **(B)** *grh-GFP* eye discs. Scale Bar 40μm.

(C-D) w^{1118} eye discs treated with **(C)** and without tyramide **(D)**. Scale Bar 40μm.

(E) Fluorescent intensity comparison between tyramide amplified eye discs and non- tyramide amplified eye discs. All images were taken using the same microscope settings. (Tyramide treated: *grh-GFP* n=3, w^{1118} n=3. Non-tyramide treated: *grh-GFP* n=2, w^{1118} n=2.)

Supplementary Figure 3. grh^{WG} MARCM Clones are also lost

A-B) Confocal images of control **(A)** and grh^{WG} **(B)** MARCM clones maintained at 25C. Scale Bar 40μm.

C) Quantification of the number of clones per midgut in control (6DPCI: n= 18 midguts 10DPCI: n=26 midguts) and grh^{WG} (6DPCI: n=15 midguts, 10DPCI: n=26 midguts) MARCM clones at 6DPCI and 10DPCI. A reduction in the number of clones in grh^{WG} midguts is observed at both time points quantified. (Mean ± SEM, One-Way ANOVA with Tukey's Test, ***p=0.0009, ****p<0.0001).

D) Quantification of clonal size between control and grh^{WG} MARCM clones. At both 6DPCI and 10DPCI, grh^{WG} clonal size, measured by counting the number of cells per clone is smaller than that of control clones. Control – 6DPCI: n=754 clones, 18 midguts; 10DPCI: n=1169 clones, 26 midguts. grh^{WG} – 6DPCI: n=242 clones, 15 midguts; 10DPCI: n=499 clones, 26 midguts. (Mean ± SEM, One-Way ANOVA with Tukey's Test, ***p=0.0002, ****p<0.0001).

Supplementary Figure 4. grh^{370} MARCM clones affect ISC proliferation and differentiation

A) Control clones are larger in size compared to *grh* mutant clones at 10DPCI. Clonal size was calculated by counting the number of cells within each clone in control and *grh* mutants. Control – n= 770 clones, 26 midguts. grh^{S2140} – n= 526 clones, 15 midguts. grh^{IM}- n=554 clones, 21 midguts. grh^{370} – n=269 clones, 25 midguts. (Mean ± SEM, One-Way ANOVA with Tukey's Test, ***p=0.0002, ****p<0.0001).

B) Quantification of the cellular composition of MARCM clones immunostained with Prospero and Pdm-1. The number of ECs (GFP+ Pdm-1+) , EE cells (GFP+ Prospero+) and ISC/EBs (GFP+)

for control and *grh* mutant clones was quantified for each genotype and percentage values calculated. (χ^2 Test, control vs. grh^{S2140} p=0.8325, control vs grh^{IM} p=0.8650 and control vs. grh^{370} ****p<0.0001).

Supplementary Figure 5. Loss of grh does not affect junctional proteins

A-C) Confocal images of control and *grh* mutant MARCM clones immunostained with septate junction Coracle. Scale Bar 40μm.

D) Quantification of fluorescent intensity levels between clonal cells in control and *grh* mutant clones. A ratio of fluorescent intensity was calculated by measuring Cora fluorescent intensity in clonal cells and dividing it by intensity in non-clonal cells. Control – n= 56 clones, 2 midguts. grhS2140 – n=75 clones, 4 midguts. grhIM – n=102 clones, 4 midguts. (Mean ± SEM, One-Way ANOVA with Tukey's Test, ns = not significant).

E-G) Representative images of control and *grh* mutant MARCM clones. These midguts were immunostained with junctional protein Dlg. Scale Bar 40μm.

H) Quantification of Dlg fluorescent intensity levels in control and *grh* mutant MARCM clones. The fluorescent intensity was calculated as a ratio between clonal and non-clonal cells. Control – n= 134, 5 midguts. grhS2140 – n= 102 clones, 3 midguts. grhIM – n=136 clones, 5 midguts. (Mean ± SEM, One-Way ANOVA with Tukey's Test, ns = not significant).

I) Quantification of Arm fluorescent ratio between clonal and non-clonal cells of control and *grh* mutant clones. Control – n= 52 clones, 2 midguts. grh^{S2140} – n=67 clones, 3 midguts. grh^{IM} – n= 60 clones, 3 midguts. (Mean ± SEM, One-Way ANOVA with Tukey's Test, ns = not significant).

Supplementary Figure 6. Over expression of grh.RL in ISC/EBs results in cell death

A-C) Confocal images of control midguts **(A)**, midguts over expressing N-isoform, grh.RP **(B)** and midguts ectopically expressing O-isoform, grh.RL **(C)** in ISC/EBs. Whereas activated caspase 3 was not detected in control and *esg^{TS}> UAS-grh.RP* midguts, it was observed in *esg^{TS}> UAS-grh.RL* midguts. Scale Bar 40μm.

D) Representative image of midgut expressing cell death gene, *reaper* in ECs and immunostained with activated caspase 3 for a positive control. Scale Bar 40μm.

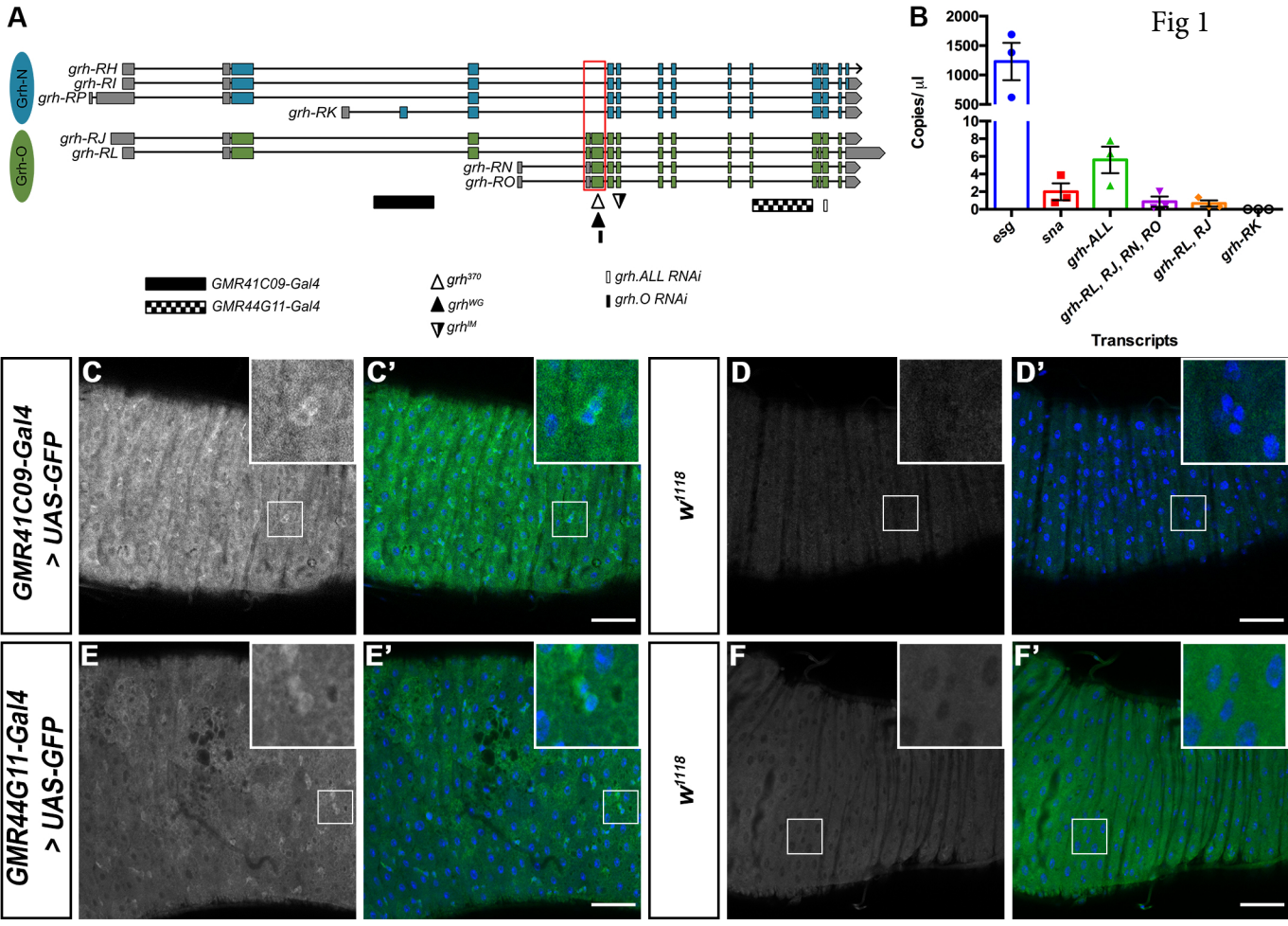
A
Grh-N
Grh-O
grh-RH
grh-RI
grh-RP
grh-RK
grh-RJ
grh-RL
grh-RN
grh-RO
GMR41C09-Gal4
GMR44G11-Gal4
grh370
grhWG
grhIM
grh.ALL RNAi
grh.O RNAi
B
Fig 1
Copies/ µl
2000
1500
1000
500
10
8
6
4
2
0
esg
sna
grh-ALL
grh-RL, RJ, RN, RO
grh-RL, RJ
grh-RK
Transcripts
GMR41C09-Gal4 > UAS-GFP
GMR44G11-Gal4 > UAS-GFP
w1118
w1118
C
C'
D
D'
E
E'
F
F'

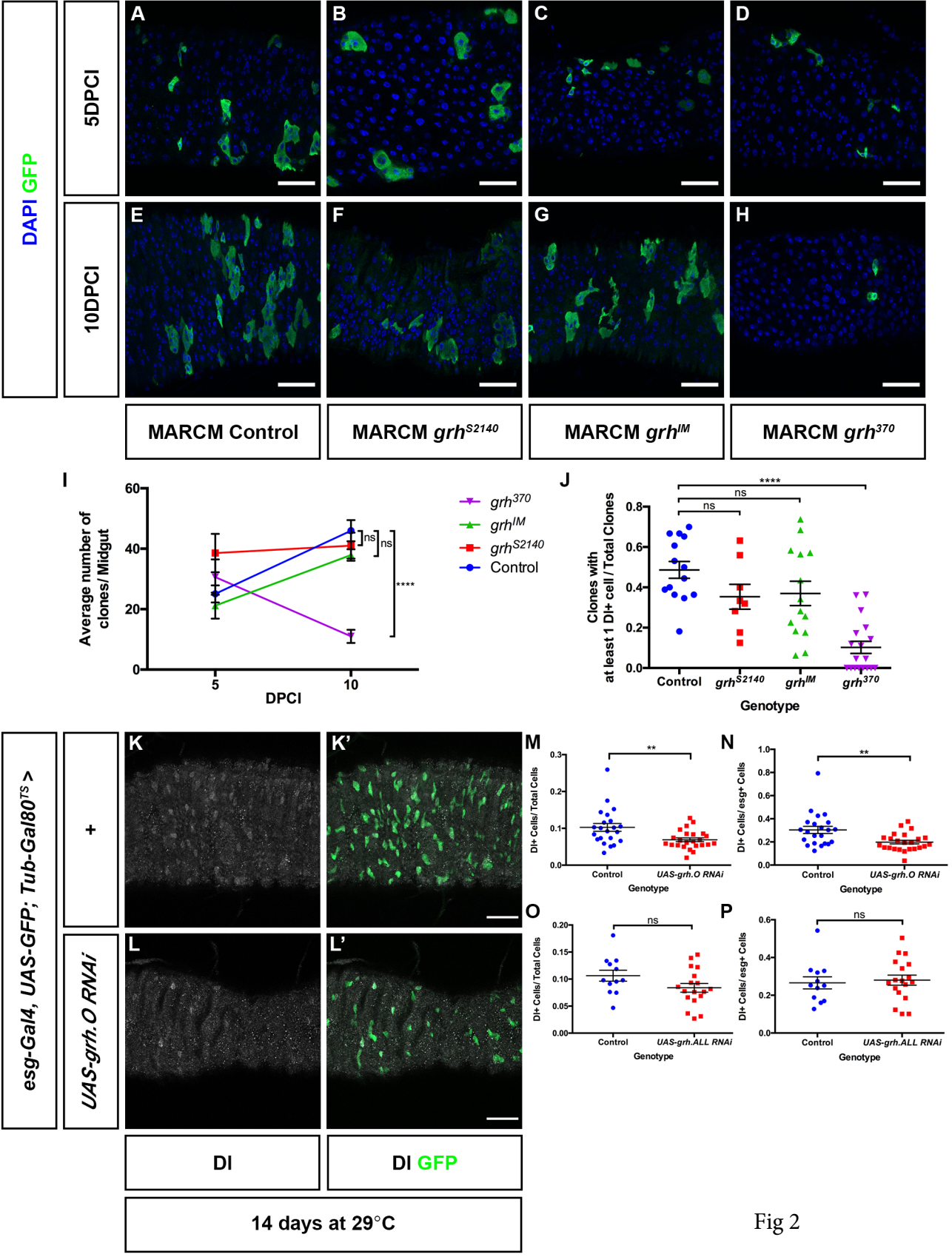
DAPI GFP
5DPCI
10DPCI
A
B
C
D
E
F
G
H
MARCM Control
MARCM grhS2140
MARCM grhIM
MARCM grh370
I
Average number of clones/ Midgut
DPCI
grh370
grhIM
grhS2140
Control
ns
****
J
Clones with at least 1 DI+ cell / Total Clones
Genotype
Control
grhS2140
grhIM
grh370
esg-Gal4, UAS-GFP; Tub-Gal80TS >
+
UAS-grh.O RNAi
K
K'
L
L'
DI
DI GFP
14 days at 29°C
M
N
O
P
DI+ Cells/ Total Cells
DI+ Cells/ esg+ Cells
UAS-grh.O RNAi
UAS-grh.ALL RNAi
**
ns

Fig 2

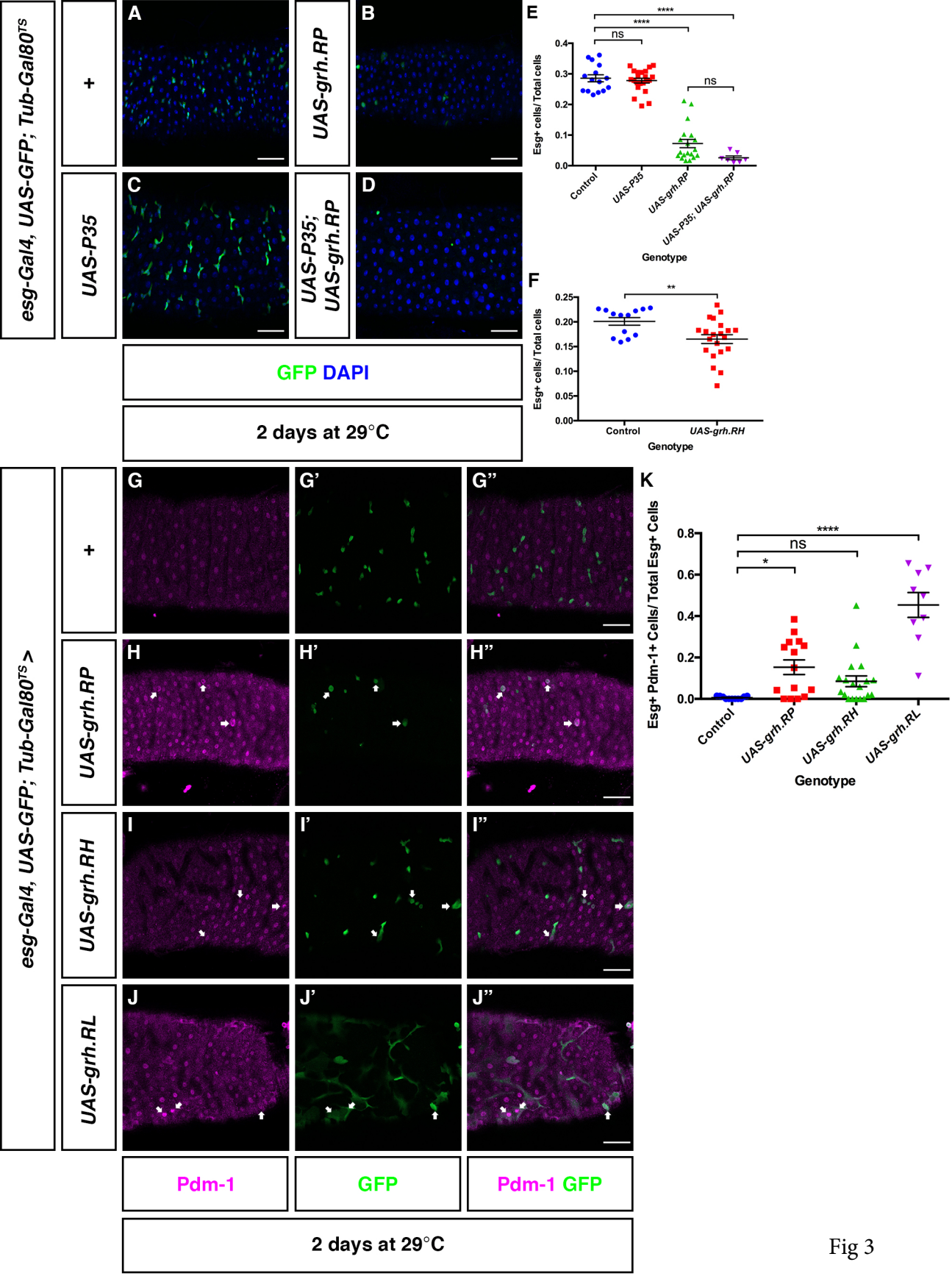
esg-Gal4, UAS-GFP; Tub-Gal80TS
+
UAS-P35
UAS-grh.RP
UAS-P35; UAS-grh.RP
A
B
C
D
GFP DAPI
2 days at 29°C
E
Esg+ cells/ Total cells
Control
UAS-P35
UAS-grh.RP
UAS-P35; UAS-grh.RP
Genotype
ns
****
F
Esg+ cells/ Total cells
Control
UAS-grh.RH
Genotype
**
esg-Gal4, UAS-GFP; Tub-Gal80TS >
UAS-grh.RP
UAS-grh.RH
UAS-grh.RL
G
G'
G''
H
H'
H''
I
I'
I''
J
J'
J''
Pdm-1
GFP
Pdm-1 GFP
2 days at 29°C
K
Esg+ Pdm-1+ Cells/ Total Esg+ Cells
Control
UAS-grh.RP
UAS-grh.RH
UAS-grh.RL
Genotype
ns
*
****

Fig 3

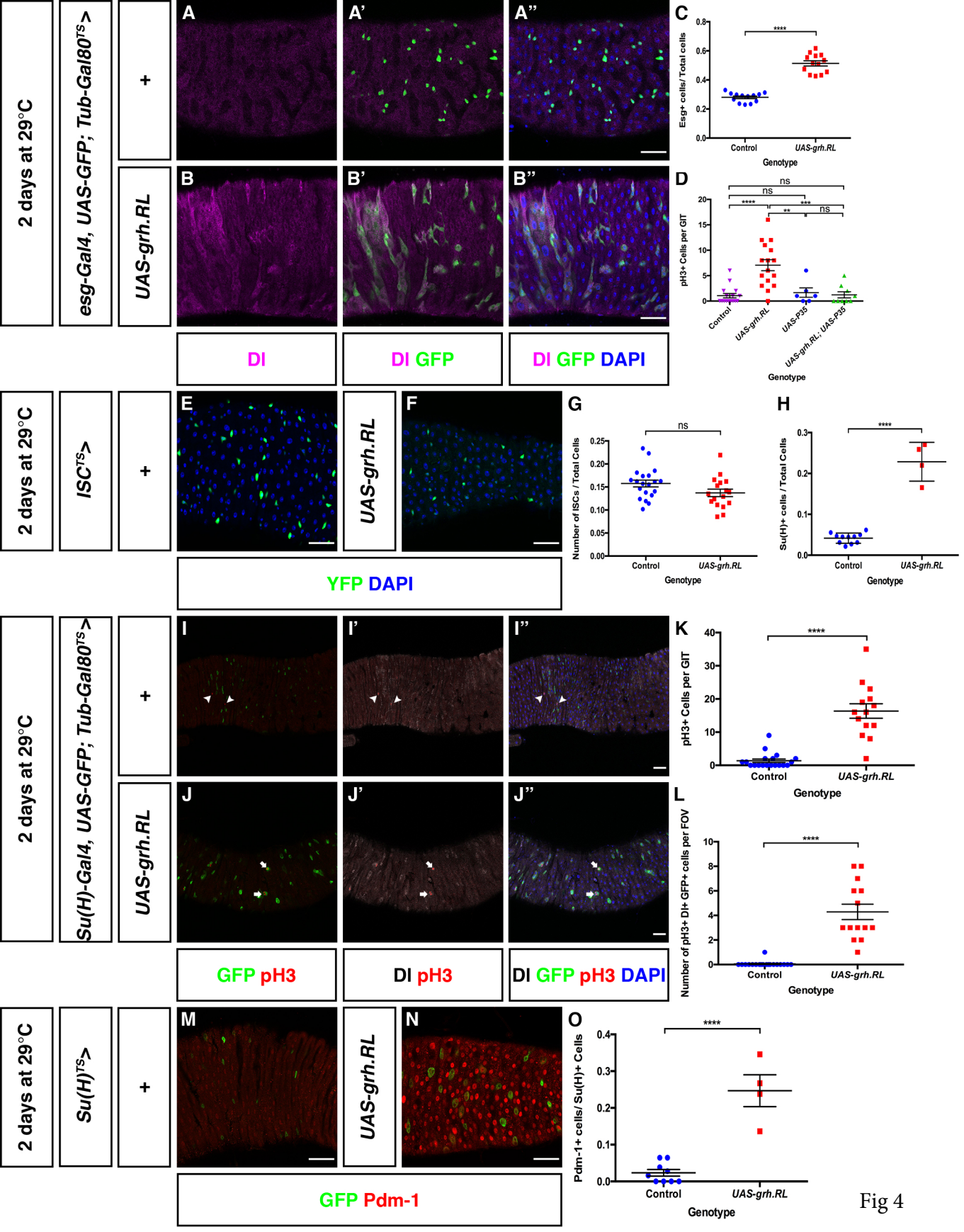
2 days at 29°C
esg-Gal4, UAS-GFP; Tub-Gal80TS>
+
UAS-grh.RL
A
A'
A''
B
B'
B''
C
Esg+ cells/ Total cells
Control
UAS-grh.RL
Genotype
D
pH3+ Cells per GIT
Control
UAS-grh.RL
UAS-P35
UAS-grh.RL; UAS-P35
Genotype
Dl
Dl GFP
Dl GFP DAPI
2 days at 29°C
ISCTS>
+
UAS-grh.RL
E
F
G
Number of ISCs / Total Cells
Control
UAS-grh.RL
Genotype
H
Su(H)+ cells / Total Cells
Control
UAS-grh.RL
Genotype
YFP DAPI
2 days at 29°C
Su(H)-Gal4, UAS-GFP; Tub-Gal80TS>
+
UAS-grh.RL
I
I'
I''
J
J'
J''
K
pH3+ Cells per GIT
Control
UAS-grh.RL
Genotype
L
Number of pH3+ Dl+ GFP+ cells per FOV
Control
UAS-grh.RL
Genotype
GFP pH3
Dl pH3
Dl GFP pH3 DAPI
2 days at 29°C
Su(H)TS>
+
UAS-grh.RL
M
N
O
Pdm-1+ cells/ Su(H)+ Cells
Control
UAS-grh.RL
Genotype
GFP Pdm-1

Fig 4

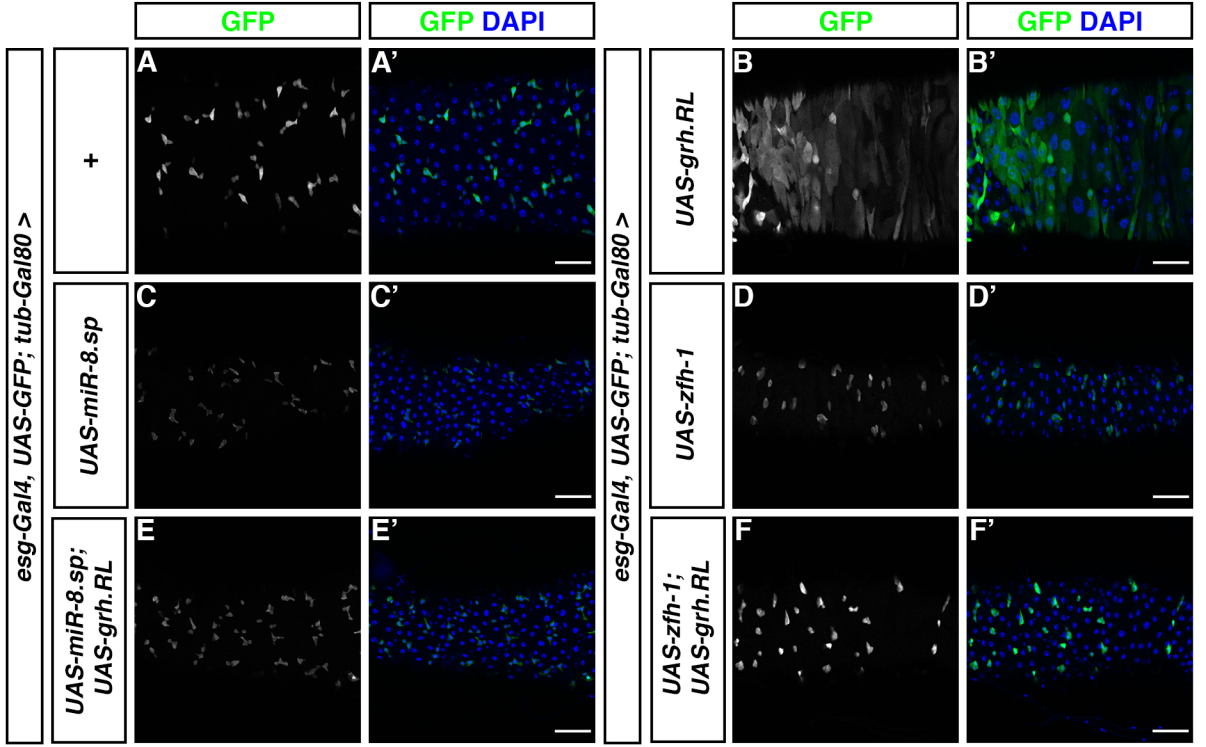
GFP
GFP DAPI
esg-Gal4, UAS-GFP; tub-Gal80 >
+
UAS-miR-8.sp
UAS-miR-8.sp; UAS-grh.RL
UAS-grh.RL
UAS-zfh-1
UAS-zfh-1; UAS-grh.RL
A
A'
B
B'
C
C'
D
D'
E
E'
F
F'

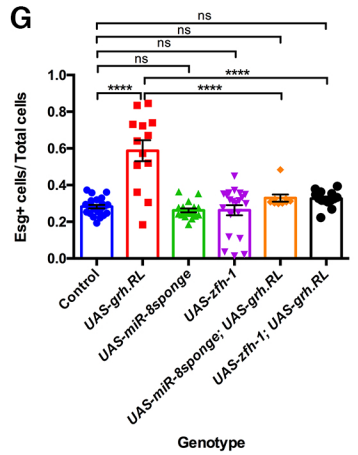
G
Esg+ cells/ Total cells
1.0
0.8
0.6
0.4
0.2
0.0
ns
ns
ns
ns
****
****
****
Control
UAS-grh.RL
UAS-miR-8sponge
UAS-zfh-1
UAS-miR-8sponge; UAS-grh.RL
UAS-zfh-1; UAS-grh.RL
Genotype

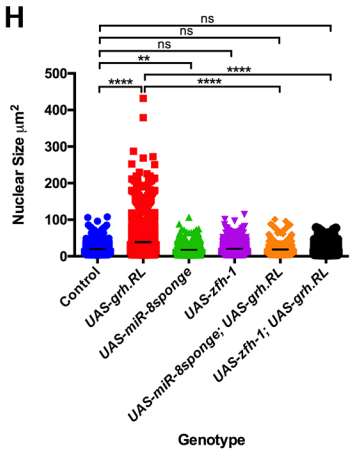
H
Nuclear Size μm2
500
400
300
200
100
0
ns
ns
ns
**
****
****
****
Control
UAS-grh.RL
UAS-miR-8sponge
UAS-zfh-1
UAS-miR-8sponge; UAS-grh.RL
UAS-zfh-1; UAS-grh.RL
Genotype

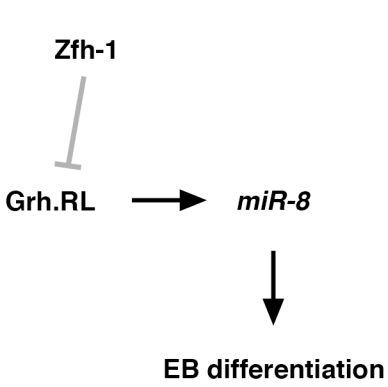
I
Zfh-1
Grh.RL
miR-8
EB differentiation

Fig 5